Discrete Chaotic Ice Failure Model Incorporating Extrusion Effects

by
Claude Daley[1] , Jukka Tuhkuri[2] and Kaj Riska[2]

Submitted to

National Energy Board
311, 6th Avenue S.W.
Calgary, Alberta
T2P 3H2

[1] Daley R&E
64 Cochrane St.
St. John's, Newfoundland
CANADA A1C 3L6

[2] Helsinki University of Technology
Ship Laboratory
Tietotie 1, SF 02150, Espoo
Finland

Table of Contents

1. Introduction

1.1 General

Ice-structure contact can cause large local and global forces on a structure. A model of ice contact against a vertical structure is described in this report. The model is an extension of an earlier ice load model, (Daley, 1991) which was based on the concept that the formation of ice flakes defines the ice load. The main addition to the earlier model is the consideration of the extrusion of the granular crushed ice and the rubble surcharge.

The earlier ice load model is described in Chapter 2. It is shown that an ice load model based on flaking events is highly dynamics and chaotic.. The dynamics arise from the sudden drops in load, caused by the flaking. The chaos is caused by the non-linear dependence of each flake on prior flakes. While the simple flaking model is shown to be correct for certain assumptions, which may be valid in ship-ice interaction, it lacks treatment of extrusion which is a common and possibly essential aspect of ice-structure interaction.

Chapter 3 describes some field experiments which indicate the need to model extrusion effects.

Chapter 4 describes a number of candidate ways in which granular ice may be formed. The nature of the formation process will affect the nature and properties of the granular material. Uncertainty about the properties of granular ice must be considered when selecting modelling approaches.

Chapter 5 discusses how to model the mechanics of granular extrusion. Two different approaches are discussed, one more rigorous and one more simplified. It is seen that the simpler approach gives results that are well within the range of uncertainty caused by uncertainty about the properties of granular ice.

Chapter 6 describes the modified chaotic flaking model, with the inclusion of extrusion forces.

Chapter 7 shows the results of the model, sensitivities to certain model parameters.

Chapter 8 discusses the deficiencies of the new model, and describes several additional developments and experiments that would be useful refinements.

1.2 Background to the Discrete Chaotic Ice Failure Model

In 1988 the Helsinki University of Technology, together with the Wartsila Arctic Research Centre, conducted a landmark series of ice crushing tests (Joensuu and Riska, 1988). The tests revealed a number of phenomena that had not been noticed so clearly before. The most obvious aspect was that the ice-structure contact geometry was line-like. It was also observed that the force time history contained a sequence of triangles whose duration was linked to their magnitude(see Figure 1). Similar features were seen during field tests on the icebreaker SAMPO (Riska, Rantala and Joensuu, 1990). This new data called for an explanation. Daley (1991) produced the needed explanation of the Joensuu-Riska tests by

developing an ice load model based on a process of macroscopic fracture events. The new model was not based on continuum mechanics but on discrete fracture events. The model was able to provide a mechanistic and causal explanation for all the key observations; the presence of a thin line of high pressure contact, the patterns and magnitude of the force-time history, the observed pressure-area effect, the piece size distribution of broken material, and the stochastic nature (lack of repeatability) of the tests.

A number of researchers have found application for Daley's ice load process model. Kujala et. al. (1993) have applied an extended version of the approach to examine the ice load on a ship trapped in pressured ice and is equivalent in many regards to level ice acting on a wide structure.

Fransson, in examining the results of another set of ice load experiments, found that an extended version of Daley's model worked very well (Fransson et.al.1991).

The problem of ice loads on narrow dynamic structures was treated in Riska et.al. (1993) using another extension of Daley's model.

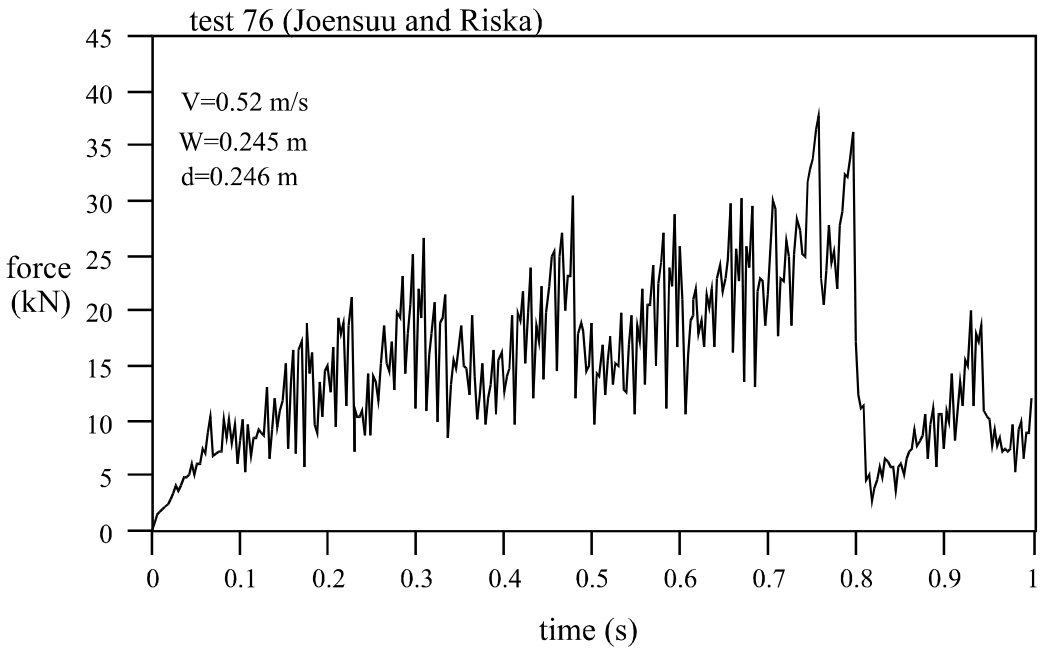

Figure 1. Force measurements from a block crushing test. (Riska and Joensuu, 1988)

2. Basic Discrete Ice Failure Model

2.1 Introduction

The basic chaotic ice failure process model (Daley 1991) assumes that the force is governed by the formation of flakes. The flakes, or spalls, remove part of the ice edge, lowering the area of ice in contact with the structure. This causes a drop in the ice load.

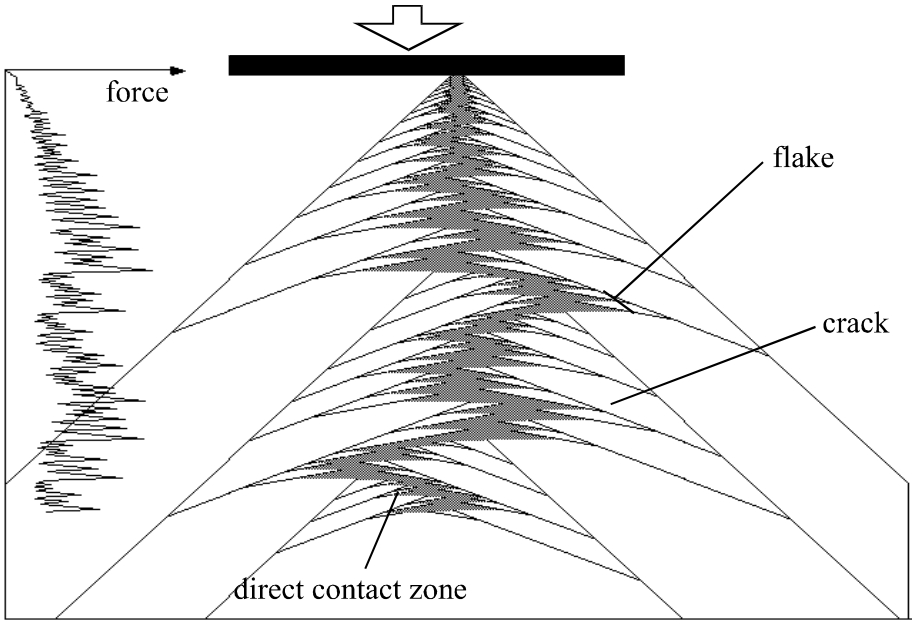

Figure 2. Contact Failure Process Model (Daley, 1991). The contact process is modelled by a discrete sequence of through-body cracks.

Figure 3 shows a comparison of the predictions made with the contact model shown in Figure 2 and results from crushing experiments(from Figure 1). It is clear that the contact model is capable of reproducing the essential behaviour seen in the crushing experiments. In doing so the model opens an entirely new way of describing and modelling the apparent randomness of ice loads. The contact model is an example of deterministic chaos. Deterministic chaos, as the name implies, starts with the premise that all the mechanics are deterministic. As the mechanical process proceeds, non-linearities in the mechanics result in a chaotic evolution. Chaotic processes are preferable to random processes as an approach to modelling a natural system, because they allow the cause of the variations to be clearly seen. Figure 4 (from Daley 1991) shows the chaotic attractor of the crushing model. The distribution of values can be described by a density function that can be precisely described. Although chaotic processes are deterministic, their exact sequence can not be exactly predicted in advance. This is because of their sensitivity to initial conditions, along with the properties of real numbers.

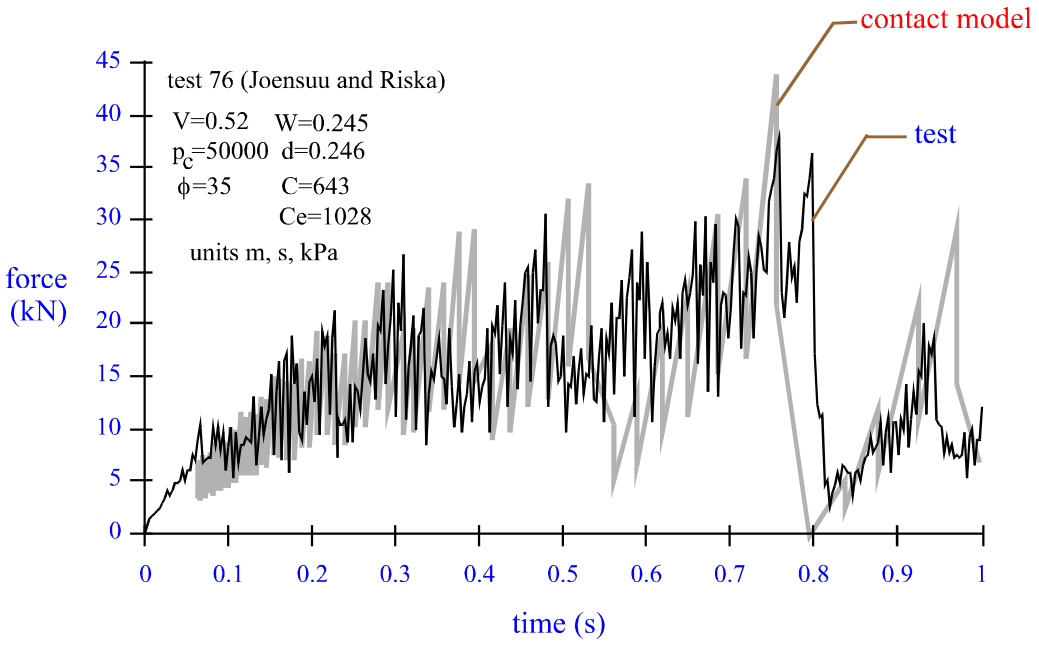

Figure 3. Comparison of model predictions with Experiments (Daley, 1991, Riska and Joensuu, 1988)

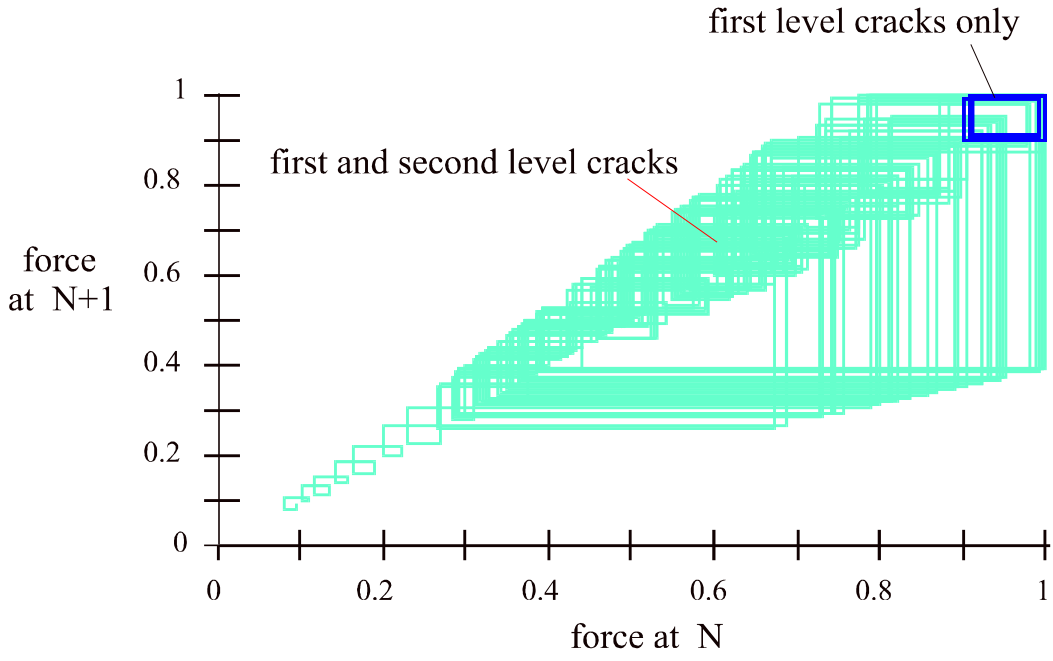

Figure 4. Two level attractor for the contact model shown in Figure 2 and Figure 3. This plot shows that the sequence of force values will never exactly repeat (from Daley 1991).

2.2 Equations Describing The Edge Cracking

The few equations governing the failure process will next be described. Figure 5 shows the parameters of the contact. The two dimensional ice wedge is assumed to have unit thickness. The contact width (L) results in a total force (F_t) on the flake of:

$$F_t = p_c \frac{L}{2} \tag{1}$$

The shear force F_s is:

$$F_s = F_t \sin\alpha = p_c \frac{L}{2} \sin\alpha \tag{2}$$

The normal force F_{nor} is:

$$F_{nor} = F_t \cos\alpha = p_c \frac{L}{2} \cos\alpha \tag{3}$$

The length of the crack (B) can be shown to be:

$$B_{cr} = \frac{\left(\frac{Y_1}{\tan\theta} - |X_1| \right)}{\cos\alpha - \frac{\sin\alpha}{\tan\theta}} \tag{4}$$

There also exists a special case when $\theta = 90°$, where:

$$B = \frac{W/2 - |X_1|}{\cos\theta} \tag{5}$$

Note that:

$$\left(\frac{Y_1}{\tan\theta} - |X_1| \right) \geq \frac{L}{2} \tag{6}$$

The situation shown in Figure 5 can only continue until the direct contact reaches point marked “e”. If a flake does not occur by then, then no flaking is possible at that level, or in other words no flakes can occur at angle α. The reason is because the stresses on all flakes of angle α will not exceed the value attained when the penetration reaches the point “e”. Thus in

the limiting case (see Figure 6) Eq. 6 becomes an equality and Eq. 4 simplifies to a critical value of B;

$$B_{cr} = \frac{L/2}{\cos\alpha - \frac{\sin\alpha}{\tan\theta}} \tag{7}$$

where α is the angle of the flake crack (to plane of contact) and θ is the angle of the edge to which the crack runs. Eq. 7 will permit the determination of critical values of shear strength.

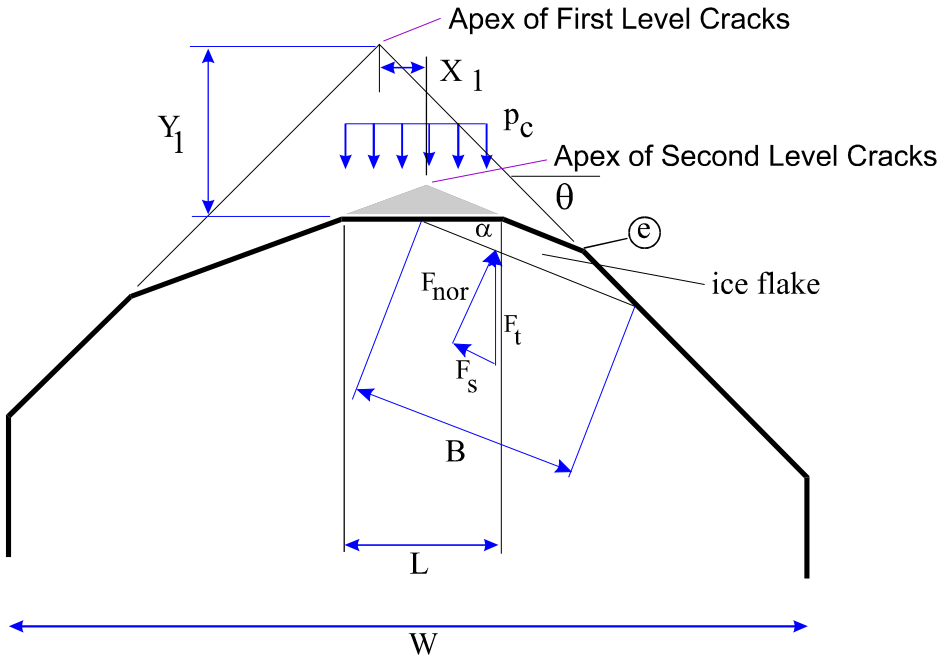

Figure 5. Flake geometry in contact model for the general case.

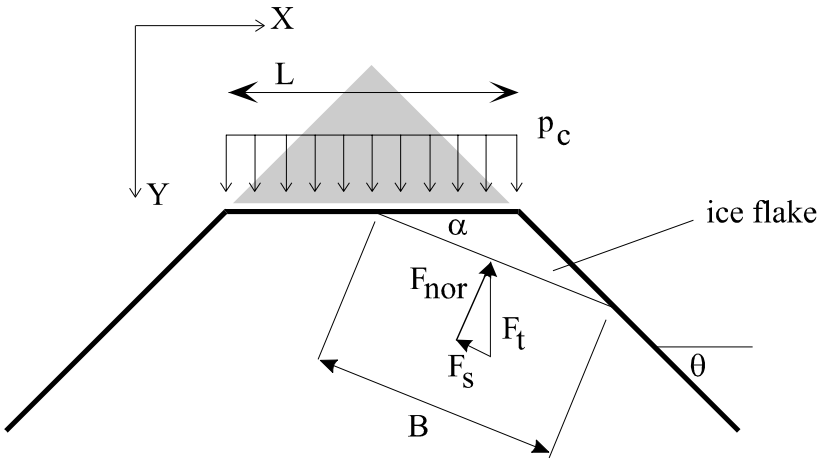

Figure 6. Flake geometry in contact model for the limiting case.

Failure will occur on the plane of the crack when the shear stress exceeds the failure value specified by the Coulomb failure criteria as:

$$c = \tau_{fail} - p \cdot \tan(\phi) \tag{8}$$

Using Eq. 2, 3 and 4, c becomes:

$$c = p_c \frac{L}{2} \frac{\left(\sin\alpha - \cos\alpha \tan\phi\right)\left|\cos\alpha - \frac{\sin\alpha}{\tan\theta}\right|}{\left(\frac{Y_1}{\tan\theta} - \left|X_1\right|\right)} \tag{9}$$

or in the simple case of $\theta = 90°$, using Eq. 5:

$$c = p_c \frac{L}{2} \frac{\left(\sin\alpha - \cos\alpha \tan\phi\right)\left|\cos\alpha\right|}{\left(W/2 - \left|X_1\right|\right)} \tag{10}$$

The maximum shear will occur at specific angles when:

$$\frac{d}{d\alpha}\left(\sin\alpha - \cos\alpha\tan\phi\right)\left(\cos\alpha - \frac{\sin\alpha}{\tan\theta}\right) = 0 \tag{11}$$

Using standard trigonometric transformations:

$$\cos 2\alpha = \frac{\sin 2\alpha}{\tan\left|\theta + \phi\right|} \tag{12}$$

which gives:

$$\tan\left|\theta + \phi\right| = \tan 2\alpha \tag{13}$$

resulting in:

$$\alpha = \frac{\theta + \phi}{2} \tag{14}$$

Eq. 14 means that cracks on a given level (see Figure 7) will run at an angle dependant on the angle of the edge to which they run. Starting with a boundary at a given angle (90° in Figure 7) Eq. 14 results in a simple sequence of angles. For the simplest case of geometry considered with $\phi = 0°$ (this being the Tresca failure criterion), all cracks will run at the angles $\theta/2, \theta/4, \theta/8$.... For $\beta = 10°$, $\theta = 90°$, $\alpha = 50°, 30°, 20°$,... The sequence of angles is finite, dependent on the highest level of flakes possible.

To examine the general behaviour of the system, the strength parameter c is normalised by the direct contact pressure:

$$k = \frac{c}{p_c} \tag{15}$$

When the flaking strength is very high, compared to the direct contact pressure, no flakes occur, only full width direct contact. There is a critical value of strength, below which flakes will occur. The quantity k (normalised strength) also has a critical value. For the case of $\theta = 90°, \beta = 0°$, k must be less than 0.5 for 45° flakes to occur.

Flakes that run to the vertical edge of the ice block are defined as first level flakes. Second level flakes are those that run to the edges created by the first level flakes (see Figure 7). The simplest case for second level flakes has $\theta = 45°$, $\alpha = 22.5°$. Each level of flake runs to the edge created by the lower level. A given level of flake will only occur if the shear strength is sufficiently low, that is, below the critical value for that level of flake.

Critical values of k (k_{cr}) can be determined as a general function of the variables α, β, θ. Eq. 8 is used with B_{cr} from Eq. 7 instead of B to give:

$$c_{cr} = p_c = \left|\sin\alpha - \cos\alpha\tan\alpha\right|\left(\cos\alpha - \frac{\sin\alpha}{\tan\theta}\right) \tag{16}$$

and by using Eq. 15:

$$k_{cr} = \frac{c_{cr}}{p_c} = \left|\sin\alpha - \cos\alpha\tan\alpha\right|\left(\cos\alpha - \frac{\sin\alpha}{\tan\theta}\right) \tag{17}$$

which gives the values shown in Table 1. The values of ϕ = 0° and ϕ = 35° are only illustrative.

Table 1. Critical values of k_{cr} vs. flake angle α and friction angle ϕ. For ϕ= 35°, the first level cracks (62.5°) form if k is less than 0.2603, for second level cracks (48.75°), k < 0.0777 and so on. With increasing ϕ, the crack angles become larger, while k_{cr} values decrease .

ϕ=0 °			ϕ=35 °		
θ°	α°	k_{cr}	θ°	α°	k_{cr}
90	45	0.5	90	62.5	0.2603
45	22.5	0.2071	62.5	48.75	0.0777
22.5	11.25	0.0995	48.75	41.8	0.0231
11.25	5.625	0.0492	41.8	38.4	0.0064

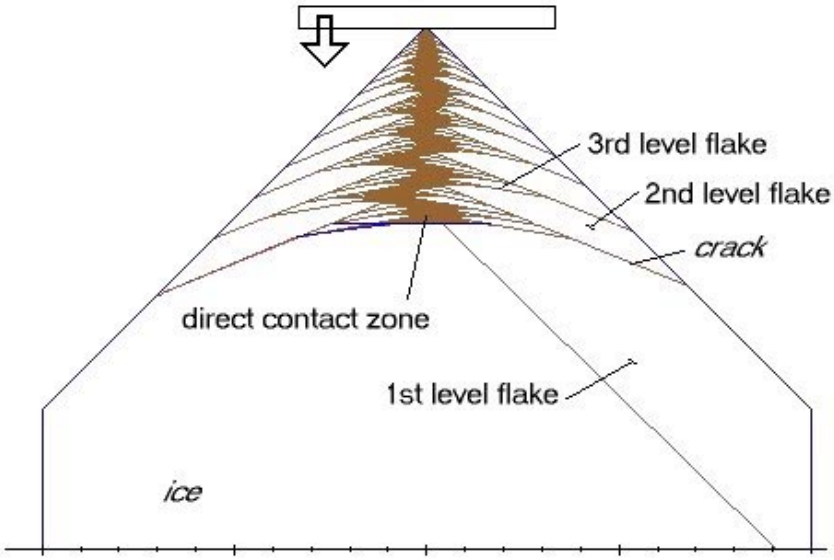

Figure 7. Definition of hierarchy of flakes.

3. Need for Extrusion Effects

The model described above was limited by certain assumptions which were appropriate in the case of the tests of Joensuu and Riska (1988). All flakes were assumed to fly freely away, so that no granular material was left to be treated. A related assumption was that only through-body cracks were considered, and all cracks were considered to leave the ice in a state of quasi-static balance.

A number of experiments have shown the above assumptions do not always hold. Tests often reveal the presence of granular material trapped in the ice-structure interface, and non-through-body cracks in the ice. Calculations suggest that the magnitude of damage experienced on ships is inconsistent with the load being solely due to a narrow straight line of direct contact. Either the line is longer (more branched and convoluted) or the pulverised ice transmits a significant portion of the force. In field situations, such as at the Molikpaq, a large pile of pulverised material can be seen in the interaction zone (see for instance Sanderson, 1988). In the medium scale indentation (MSI) tests (Frederking et al 1990 and Sandwell, 1992), a significant layer of pulverised material was seen (Figure 8). Tests by Tuhkuri (Tuhkuri and Riska, 1990) of ice extrusion and ice crushing have suggested that the extrusion of granular materials can be a significant aspect of the ice load process. Tests at the Technical Research Centre of Finland (Muhonen et. al. 1992) have also raised questions, both because of the presence of non-through-body cracks and the clear presence of granular material.

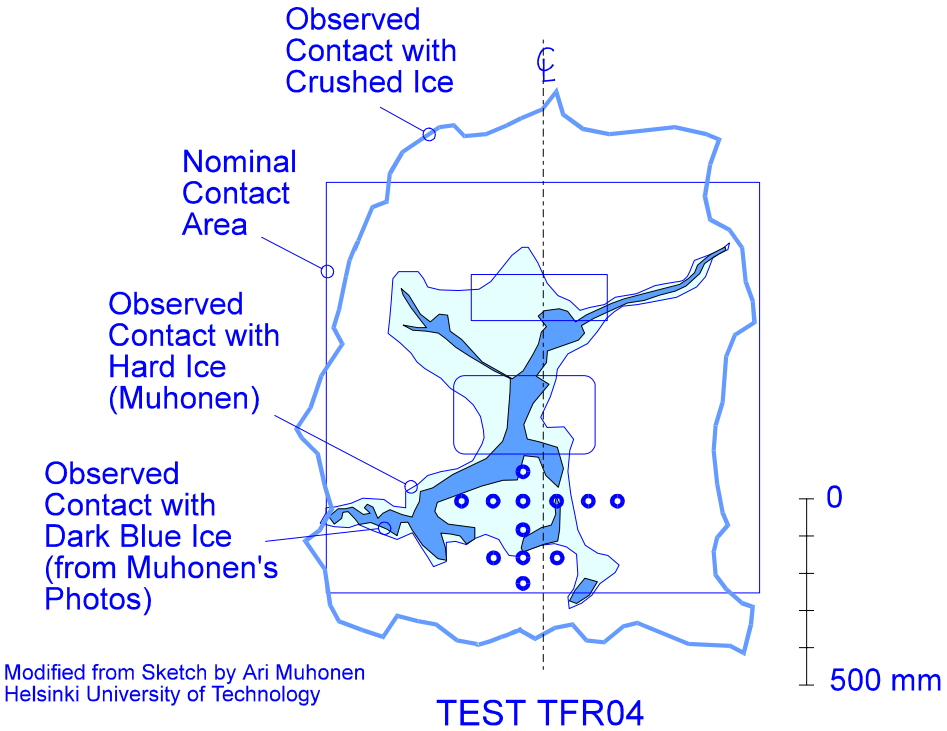

Figure 8. Direct and Crushed Ice Contact Geometry from Hobson's Choice Test TFR04 (taken from Muhonen 1991)

It has been shown that a dry granular material will normally follow Mohr-Coulomb behaviour. This is a simple linear model for shear failure and flow. Mohr-Coulomb assumes that the material is a continuum. This assumption may be invalidated if large pieces are in the flow. Nevertheless, it is best to begin by assuming Mohr-Coulomb properties for the granular material. Other authors have examined the possibility of using viscous model to describe the extrusion of crushed ice, particularly when the granular ice is experiencing high confinement pressures and may be undergoing re-crystallisation. (Singh et.al. 1995).

It is important to know what effect the pulverised material has on the interaction forces. In the MSI tests there were zones of direct contact and zones of contact with pulverised ice. The pressure distribution in the pulverised ice has been studied experimentally by Tuhkuri & Riska (1990) and shown to grow exponentially with distance from a free edge. Savage (1989) arrives at a similar conclusion based on numerical simulations of the extrusion of granular ice.

Figure 9 illustrates the point about the significance of extrusion. In Figure 9(a) and (b), the local ice failure is compared with and without consideration of the pulverised material. Two important changes occur when the pulverised material is considered. First, the force on the structure is transmitted through both the direct high pressure contact and through the pulverised ice. Secondly, and more importantly, the local stress regime in the ice is significantly changed due to the pressure distribution in the pulverised zone. It would seem that local flakes would be more difficult to form due to the confining stress of the pulverised material. One of the authors, in an analysis of crack formation (Tuhkuri, 1996, p86) has shown that a pressure of 0.5 Mpa acting on both sides of the contact area will close the surface cracks and thus significantly hinders their growth.

As the interaction shown in Figure 9(b) proceeds the width of the interaction zone will grow and the average pressure in the zone will grow. This process is limited by larger cracks as shown in Figure 9(c) and (d). The large cracks, call them global to distinguish from the local cracking in Figure 9(a) and (b), will limit the build up of force, pressure and contact width. The global crack is much less influenced by the local contact stresses. It is almost solely dependent on the total force in the contact zone, and therefore not influenced by the extrusion process.

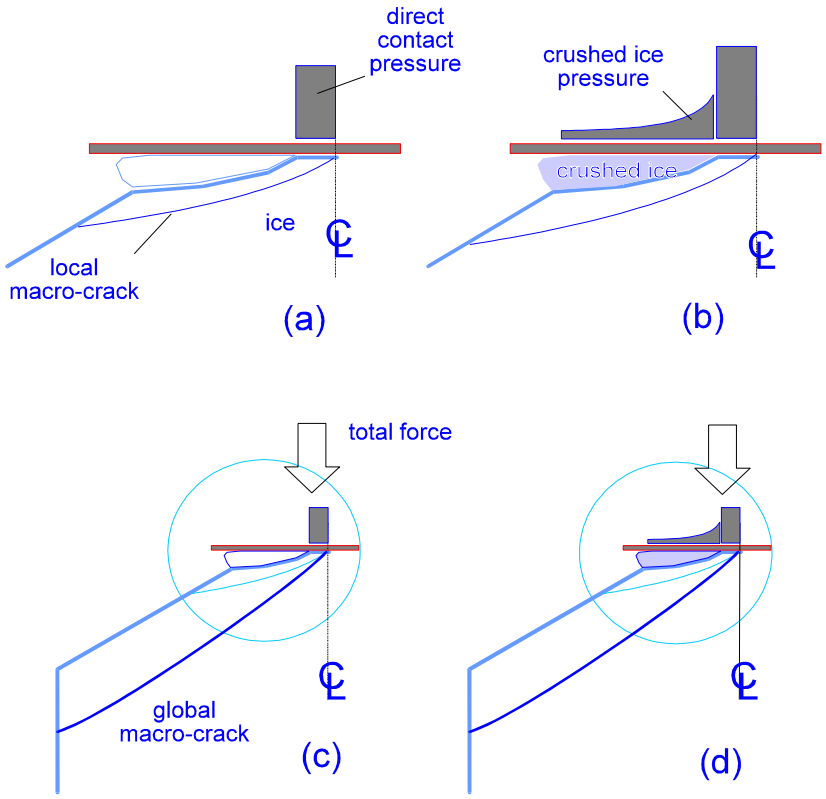

Figure 9. Local and Global Effects of Extrusion on Ice Edge Cracking and Loads.

According to the model given in Daley (1991) the global crack would be termed a Level I crack, while the local cracks would be termed Level II and higher. Daley (1991) did not consider the effects of extrusion on the process.

The MSI tests produced some interesting and relevant results. Figure 10 illustrates the evolution of pressure vs. area during test TFR02. There are two opposing tendencies. There are 4 major peaks (a, b, c, d) which are each followed by a substantial drop in average pressure. Each drop is followed by a period of generally rising pressure until the next major peak and drop. It is speculated that each major peak/drop represents a major or global crack. Between these major cracks there are numerous minor cracks, with a build-up of the extrusion pressures.

This data raises several important questions that will be addressed:

- What is the nature of the global cracks that is permitting the average pressure to drop?
- Is extrusion the cause the cause of the rise in pressures between major cracks?
- Could certain geometry preclude the development of the global cracks and allow the average pressures to continue to rise with area?
- In Figure 10 the maximum capacity (12MN) of the MSI system is shown. How would the pressures change in interactions of much higher force? Would the same trends continue?

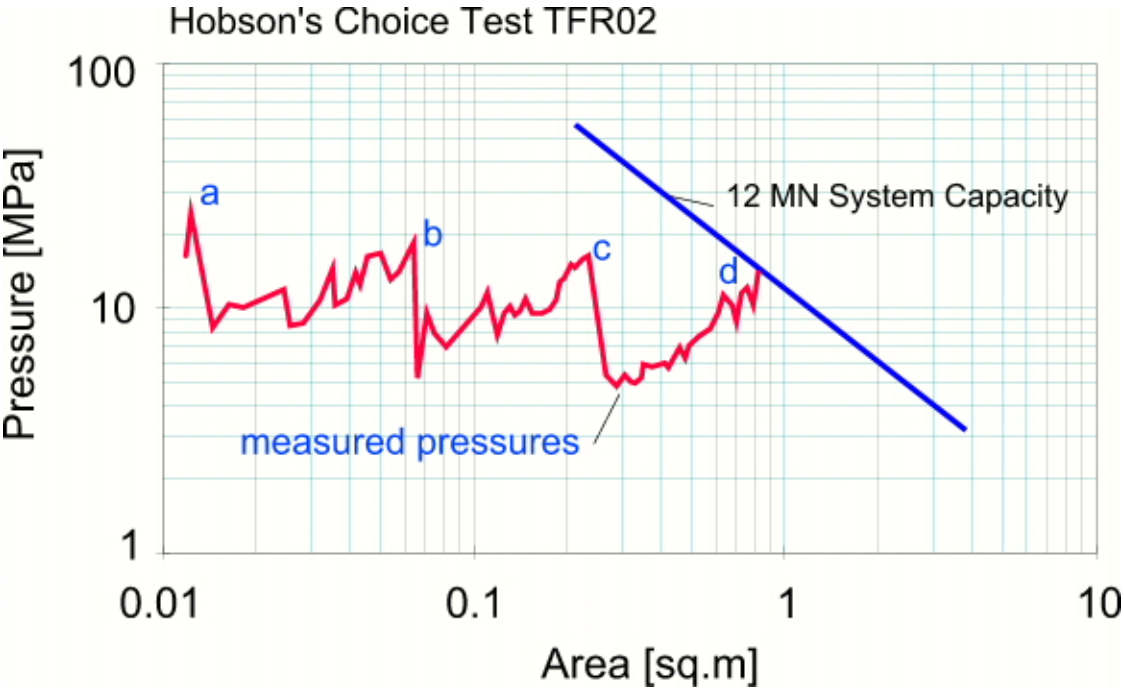

Figure 10. The Pressure-Area Relationship during the Hobson's Choice Ice Indentation Test TFR 02

4. Formation of Granular Material

While it is clear that the granular material may be an important aspect of the ice-structure interaction process, it is not yet clear how the pulverised ice is formed. In general terms the granular material results from "crushing", but this offers no explanation of how "crushing" occurs. There are at least 4 candidate mechanisms that will produce pulverised ice. These are:

(i) the growth and coalescence of micro-cracks will produce granular material. This idea follows damage mechanics reasoning.

(ii) macro-cracks result in the rapid release of stress, and the resulting tension waves cause breakup of the material. There is laboratory evidence that stress release can result in this type of fracturing.

(iii) macro cracks allow relatively large fragments to be released into the flow of granular material. During extrusion, comminution (repeated breakup due to successive ice-ice interactions) will produce the fine granular material. This process will result in a wide variety of piece sizes (see Tuhkuri,1994). Cross sections taken from the MSI tests suggest that this mechanism was taking place.

(iv) a cascade of macro cracks takes place to rapidly reduce a large fragment or zone into rubble. This would occur if a single crack were insufficient to relax the stresses. After the cascade, presumably comminution would take place. This is a new idea supported by experimental observations (Tuhkuri, 1994). Tuhkuri (1996) has shown by using computational fracture mechanics that if a population of surface cracks is assumed, the growth of the first crack is followed rapidly by growth of the other cracks. Such a process can be described as a cascade of flakes. A cascade of flakes has been proposed as a model for ice failure by Daley, Tuhkuri and Riska (1994)

The authors believe that all four of these mechanisms can be active depending on the interaction conditions. For example, if the growth of macro cracks is hindered by high confinement, only micro cracking may occur and the mechanism (i) is the active one. All four could be active at various times during an interaction.

5. Models of Extrusion

5.1 Introduction

The case under consideration consists of a vertical structure, a sloping ice face (due to the flakes) and granular ice being extruded upwards and downwards. A rubble pile is formed above and below the ice sheet, which causes a restraint pressure at the exit to resist the extrusion. Figure 11 illustrates the process that we are considering. The crushed ice is held and extruded betwee two non-parallel plates. Both gravity (and buoyancy) and friction resist the extrusion.

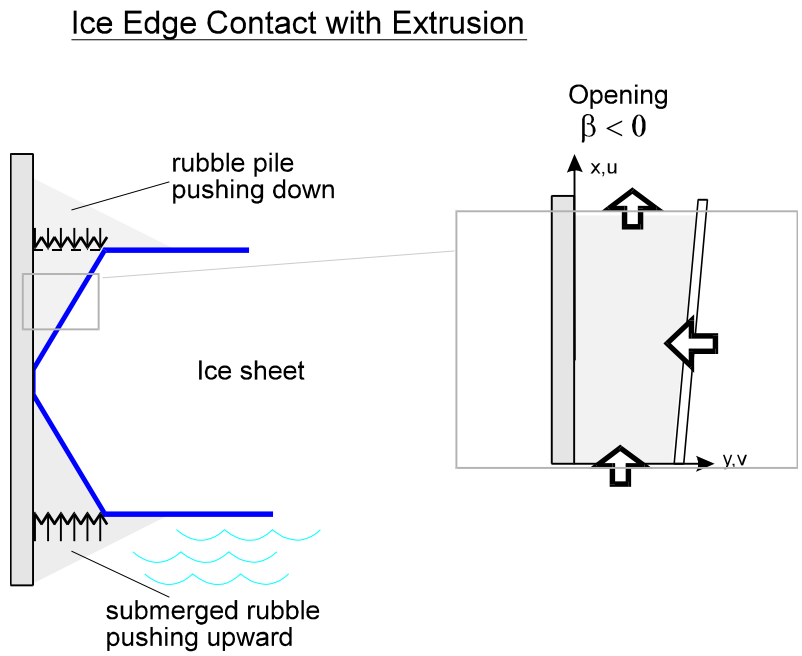

Figure 11. Overview of Contact with Extrusion.

5.2 Savage's Mohr-Coulomb Extrusion Model

5.2.1 Introduction to Savage's Model

This section introduces a calculation model developed by Savage et al. (1992) for a two-dimensional extrusion of a cohesive Mohr-Coulomb material. That model can be used to predict the pressure distribution developed during an extrusion of ice contained between two converging plates (see Figure 12).

Savage et al. (1992) have given a closed form solution for the case of extrusion between parallel plates of equal wall friction. In a general case the two plates need not be parallel and the wall frictions can have different values. The general case can also be expanded to take a pressure acting on the boundary into account (back-pressure). However, the solution of the general case is extremely lengthy in closed form and therefore it is better solved by using numerical techniques.

In the following, both the solutions given by Savage et al. (1992) are given. Then it is shown that with a proper choice of material parameters, such Mohr-Coulomb models can be used to calculate the measured pressure distribution during laboratory experiments (Tuhkuri & Riska 1994). In these experiments, crushed ice was compressed between two parallel converging plates. Then the effects of non-parallel plates and non-zero back-pressure are discussed and simple coefficients to take these two effects into account are presented. Such coefficients can be used to modify the simple closed form solution to approximate the general solution.

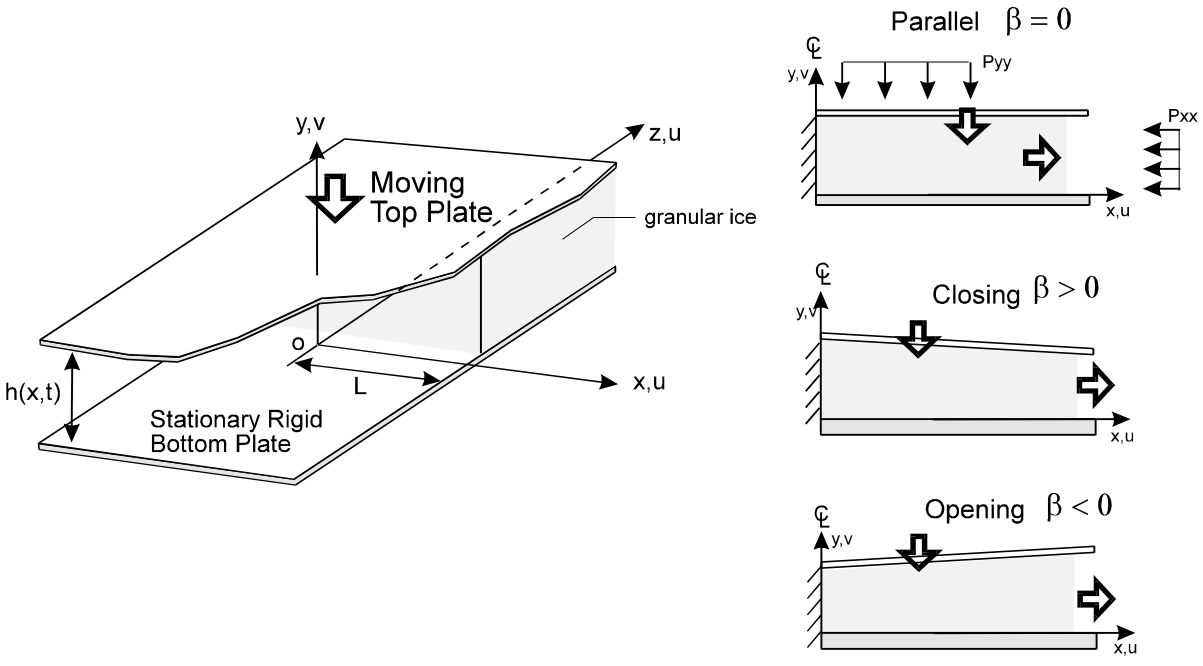

Figure 12. Horizontal extrusion mechanics.

5.2.2 Extrusion of a cohesive Mohr-Coulomb material - General case

The differential equation for the depth averaged normal stress $\bar{p}_{yy}$ in the y-direction is (Savage 1989, Savage et al. 1992)

$$\frac{\partial \bar{p}_{yy}}{\partial x} + \frac{\tan\delta_0 + \tan\delta_h}{\varepsilon \bar{k} h}\bar{p}_{yy} = -\frac{C(\tan\delta_0 + \tan\delta_h)}{\varepsilon \bar{k} h \tan\phi} - \frac{G(\tan\delta_0 - \tan\delta_h)}{2\varepsilon \bar{k}} - \frac{2Ex}{h^2 \varepsilon \bar{k}} + \frac{Ex^2}{h^3 \varepsilon \bar{k}}\frac{\partial h_0}{\partial x} \tag{18}$$

where

δ_0	wall friction angle at the bottom plate (y=0)	h(x,t)	gap height
δ_h	wall friction angle at the top plate (y=h)	$h_0(x)$	initial gap, h(x,t=0)
ρ	density	x	coordinate, see Figure 12
C	non-dimensional cohesion	t	time
ϕ	internal friction angle	L	wall length, see Figure 12
H	initial gap, h(x=0,t=0)	V	velocity of the top plate
		P	characteristic pressure
		g	9.81 m s^{-2}

The non-dimensional coefficients are

$$\varepsilon = \frac{H}{L}$$

$$E = \frac{\rho V^2}{\varepsilon P}$$

$$G = \frac{\rho g H}{P}$$

$$\bar{k} = \frac{\tan\delta_h}{2(\tan\delta_0 + \tan\delta_h)}(k_h + k_{zs}) + \frac{\tan\delta_0}{2(\tan\delta_0 + \tan\delta_h)}(k_0 + k_{zs})$$

$$k_0 = 2\left[1 - \sqrt{1 - \left(1 + \tan^2\delta_0\right)\cos^2\phi}\right] / \cos^2\phi - 1$$

$$k_h = 2\left[1 - \sqrt{1 - \left(1 + \tan^2\delta_h\right)\cos^2\phi}\right] / \cos^2\phi - 1$$

$$k_{zs} = \frac{1 - \sin\phi}{1 + \sin\phi}$$

Equation 18 is given in non-dimensional form. The x-coordinate as well as the gap height h(x,t) get therefore values between 0 and 1. Also the time is non-dimensional: at the beginning of a test t=0 and h=1, when the two plates are in contact t=1 and h=0. Hence h(t)=1-t.

It is assumed that during extrusion the material parameters C, ϕ, ρ are constants. In other words, compaction of the crushed ice is not taken into account.

If we assume that the converging plates are straight, the initial gap has the form

$$h_0(x) = 1 - \beta x \tag{19}$$

where β is the slope. A positive β gives a closing gap and a negative β an opening gap in the flow direction. When deriving the differential equation 1, it has been assumed that β<<1.

Savage et al. (1992) have used the boundary condition that the pressure p_{xx} in the flow exit is zero

$$p_{xx}\left(x = 1, y = h, t = 0\right) = 0$$

then

$$\bar{p}_{yy}\left(x = 1, t = 0\right) = \left(\frac{1 - k_h}{k_h}\right)\frac{C}{\tan\phi} + \frac{Gh}{2} \tag{20}$$

The first order differential equation 1 can be solved when the boundary condition (20) is known. The results that will be shown below were obtained by using a fourth order Runge-Kutta method. It is convenient to start from x=1 and integrate in the negative x-direction.

5.2.3 Extrusion of a cohesive Mohr-Coulomb material - Parallel plates

If we assume that $\beta = 0$ and that $\delta_0 = \delta_h = \delta$, the equations can be simplified and a closed form solution is found (Savage 1989, Savage et al. 1992)

$$\bar{p}_{yy} = \frac{B}{A^2}\left[1 - e^{A(1-x)}\right] + \frac{B}{A}\left[e^{A(1-x)} - x\right] + \frac{C}{\tan\phi}\left[\frac{e^{A(1-x)}}{k_h} - 1\right] + \frac{G}{2}(1-t)e^{A(1-x)} \tag{21}$$

where

$$A(t) = \frac{2\tan\delta}{\varepsilon\bar{k}(1-t)} \quad \text{and} \quad B(t) = \frac{2E}{\varepsilon\bar{k}(1-t)^2}$$

5.2.4 Comparison with laboratory experiments

Tuhkuri and Riska (1990, 1994) compressed crushed ice between two converging plates: an ice platen and a steel platen. Local pressures as well as the total force were measured. The measured pressure distributions were similar to those predicted by the Mohr-Coulomb model, as shown in Figure 13.

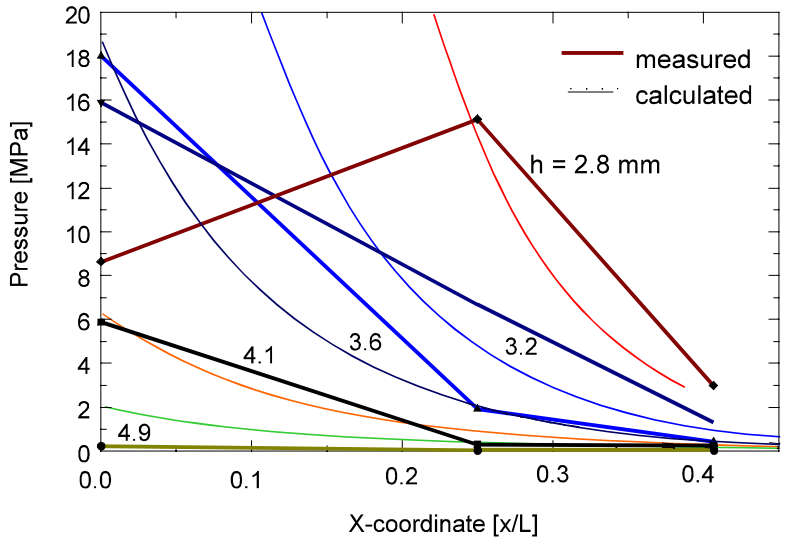

Figure 13. Pressure distribution at various layer thicknesses during test No. 21 of Tuhkuri and Riska (1994). The calculated values were obtained by using the Eq. 21. Internal friction angle was 30.5°, non-dimensional cohesion 0.0005, wall friction angle 3°, and density 448 kg/m^3.

Figure 13 suggests that the pressure distribution during extrusion of crushed ice can be predicted with the Mohr-Coulomb model, but only up to certain pressure value. This pressure limit, and the subsequent decrease of pressure at the center of the plates, can be partly explained by the gradual damaging of the ice plate used in the experiments. The extrusion pressure cannot be higher than the strength of the solid ice. However, this damage in the solid ice cannot be the whole explanation for the limit, as similar deviation from the Mohr-Coulomb model at high pressures was observed by Spencer at al. (1992), who compressed ice between two steel plates, and so the phenomenon was caused by deformations in the crushed ice. The compaction of the crushed ice into solid and the change of material properties during this compaction require further studies.

5.2.5 Non-parallel gap

In the flaking-type ice failure model described earlier in Section 2, the crushed ice formed is in an opening channel formed by the parent ice and the structure. This channel has always non-parallel sides and the extrusion pressure can be approximated with equation 18.

Figure 14 shows examples of the pressure distribution at one time instant with different values of β. The parameters used were the same as those used in Figure 13 when h=3.6 mm. In other words, the curve β = 0 gives equal pressures than the measured ones, and the curves with other β values show the calculated effect of channel closing or opening. Note that small chances in the slope have a remarkable effect on the pressure values. The same effect is shown in Figure 15. The pressures in an opening channel decrease rapidly with increasing $|\beta|$. When β = -0.1 (i.e. inclination angle $\tan^{-1}\beta$ = 5.7°) the central pressure is only about 10% of what is would be if β was zero. The value of β has no effect on the shape of exponentially decreasing $p_{yy}(x)$ curve.

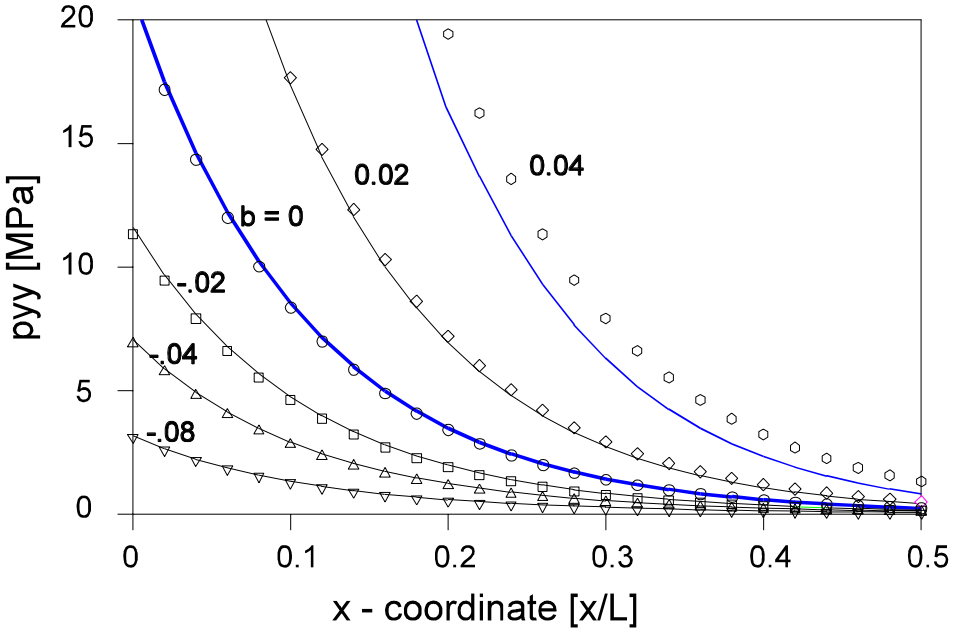

Figure 14. Pressure distribution in a non-parallel gap at one time instant with different values of β. The parameters were the same as in Figure 13 when h = 3.6 mm. Solid lines: Calculated by Eq. 18. Symbols: Calculated by Eq. 21 and 22.

The result given in Figure 15 can be used to formulate an approximate method to take the β angle into account. If we have calculated a pressure distribution $p_1(x)$ with the equation 21 we can approximate the pressure distribution in an opening channel as

$$p(x,\beta) = f(\beta)\, p_1(x) \tag{22}$$

where

$$f(\beta) = \frac{1}{(a\beta + 1)^n}$$

The constants a and n are presumably functions of boundary conditions, loading rate, temperature, scale etc. As an example, a and n were calculated for the case shown in Figure 14. a and n turned out to be functions of x-co-ordinate, but because the pressure values are small when x is zero, we are mostly interested in the small x range. The symbols shown in Figure 14 were calculated by using equation 22 together with equation 21 and a=11 and n=3.

$$a(x) = 10.43 + 8.09x \approx 11$$
$$n(x) = 3.15 - 2.88x \approx 3$$

5.2.6 Non-zero back-pressure

If the crushed ice formed accumulates on top of the breaking ice cover the weight of this rubble pile forms a non-zero pressure p_{xx} at the flow exit and the boundary condition 20 must be changed. The new boundary condition is simply

$$\bar{p}_{yy}(x=1,t=0) = p_{xx}(x=1) + \left(\frac{1-k_h}{k_h}\right)\frac{C}{\tan\phi} + \frac{Gh}{2} \tag{23}$$

Figure 16 shows the effect of pressure p_{xx} calculated by equation 18 with boundary condition 23. Again, to obtain numerical values, the test case shown in Figure 13 when h=3.6 was used as an example.

This result can again be used to formulate an approximate method to take the back pressure into account. If we have calculated a pressure distribution $p_1(x)$ without back pressure with the equation 21 we can approximate the pressure distribution as

$$p(x, p_{xxo}) = f(p_{xxo})\, p_1(x) \tag{24}$$

where p_{xx0} is the back pressure. The correction function is

$$f(p_{xx0}) = 1 + \frac{p_{xx0}}{2630}$$

where p_{xx0} is in Pa. Figure 16 shows values calculated with this approximate method.

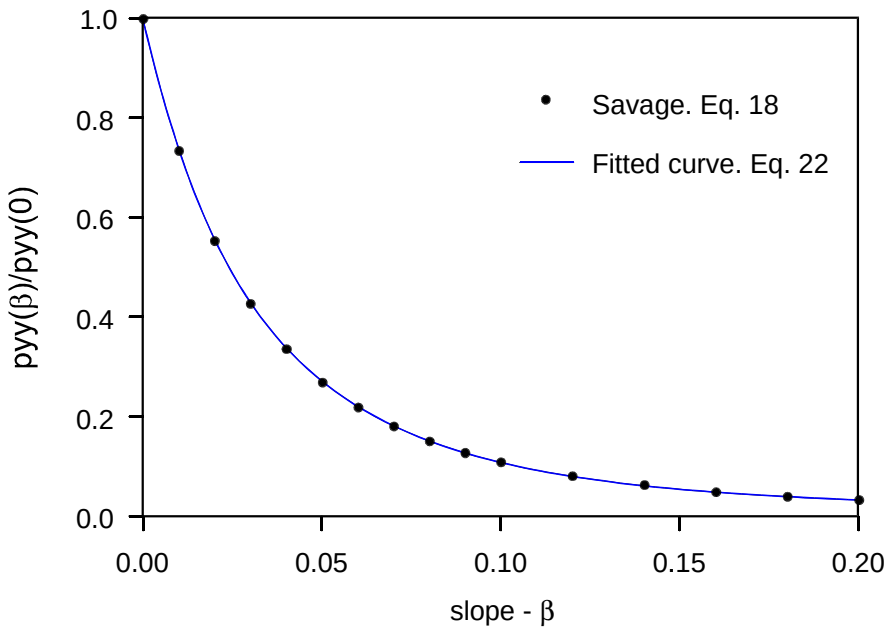

Figure 15. The central (x = 0) extrusion pressure in an opening channel. The fitted curve was obtained by using Eq. 22 with values a = 10.95 and n = 2.996.

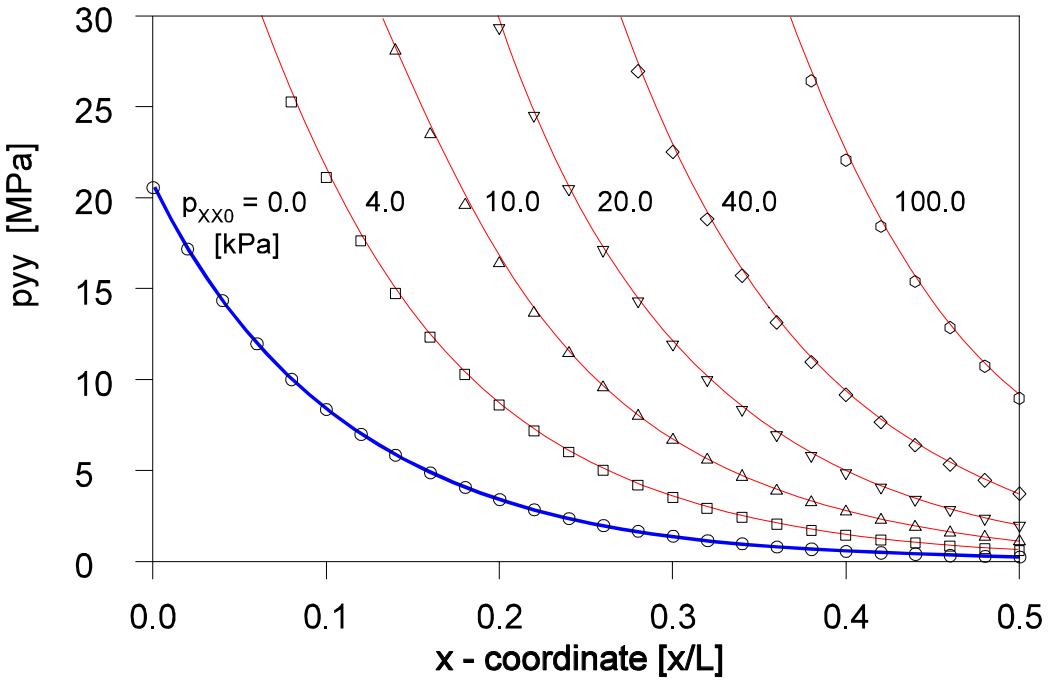

Figure 16 The effect of the back pressure p_{XX0} on the pressure distribution. Solid lines: Eq. (18) with boundary condition given in Eq. (23). Symbols: Eq. (21) with Eq. (23).

5.2.7 Summary

- It was shown that the Mohr-Coulomb solution given by Savage (1989) and Savage et al. (1992) can be used to approximate the extrusion pressures measured in small scale experiments where the converging plates were parallel.
- The general Mohr-Coulomb solution, Equation 18, can be used to calculate the pressure distribution also when the gap is opening or closing ($\beta \neq 0$) and when a non-zero back pressure (p_{xxo}) is applied. This problem has to be solved numerically.
- An approximate closed form method was formulated to analyse cases when $\beta \neq 0$ and $p_{xxo} \neq 0$ (Equations 21, 22, and 24). As an example, coefficients for this approximate method from one test case were calculated.

5.3 Simplified Extrusion Model

5.3.1 Introduction

A simplified model is now presented. The model is quite similar to that presented above, except that cohesion is not considered. There are several reasons for making this simplification. While the model presented above is more precise, it does not appear to fully describe the experimental data. The granular material appears to be much more complicated than a simple cohesive granular material. Compaction and re-solidification seem to be taking place in the center of the granular material, where the pressures have grown large. To include consideration of the solidification phenomena, which limit the extrusion pressures, it is preferable to be able to do a closed form calculation of the pressure, rather than needing to iterate to an answer. As well, in order to study the importance of extrusion in our ice-structure contact model it is necessary to be able to perform the extrusion calculations relatively quickly. The simplified extrusion equations are described below for six cases, of increasing complexity.

The equations solve the problem of ice being extruded between a vertical structure and an ice edge. There is assumed to be a layer of granular material (crushed ice) which is extruded. Above the centre of the ice the ice is extruded upwards, and forms a rubble pile above the ice. The vertical pressure at the top of the ice (which is the top of the wedge of extruding ice and the bottom of the rubble pile) is calculated from the height and density of the rubble. Below the centerline of the ice, the granular crushed ice is extruded downwards, and is resisted by friction and the buoyant forces on the rubble.

The ice is assumed to be a granular material with a lateral pressure coefficient k. This is an assumption from soil mechanics, which allows the calculation of the horizontal pressures on the structure and ice face. Using friction coefficients on both the ice and structure, the frictional forces which resist extrusion can be calculated.

The cases listed in Table 2 are considered. They build up to the 'true' condition found in loads against offshore structures. In the case of vertical extrusion, the extrusion must act against gravitational forces. The presence of a surcharge will create an initial pressure at the exit.

Table 2 Cases for Simplified Extrusion Calculations

	GEOMETRY	ORIENTATION	INITIAL PRESSURE	SKETCH
Case 1	Parallel	horizontal	pox	
Case 2	Parallel	vertical	0	
Case 3	Sloped	vertical	0	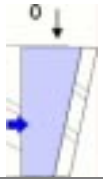
Case 4	Parallel	vertical	pox	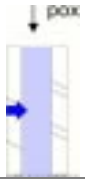
Case 5	Sloped	horizontal	pox	
Case 6	Sloped	vertical	pox	

In all the cases, the same basic differential equation is used, although terms or initial conditions will change. The derivation of the simple equation is as follows (see Figure 17) :

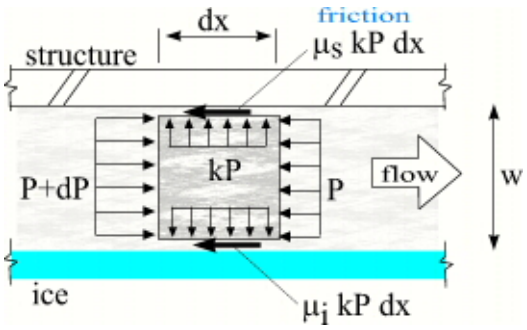

Figure 17. Sketch for derivation of simple extrusion equations.

Consider a volume of granular ice *dx* by *w* by one unit thick. The pressure on the downstream face is *P*. The pressure on the side walls is (by a simple soil analogy) *P/k* . The total frictional force on the volume is;

$$total\_friction = \frac{(\mu_i + \mu_s)}{k} \cdot P \cdot dx \tag{25}$$

so that the change in pressure across *dx* is;

$$dP = \frac{(\mu_i + \mu_s)}{k \cdot w} \cdot P \cdot dx \tag{26}$$

This is simply rearranged into the differential equation in the horizontal case;

$$\frac{\partial P(x)}{\partial x} + \frac{K \cdot P_x(x)}{w} = 0 \tag{27}$$

where K is defined below.

The differential equation in the vertical case includes the weight of the small volume and is similarly;

$$\frac{\partial P(x)}{\partial x} + \frac{K \cdot P_x(x)}{w} - \rho \cdot g = 0 \tag{28}$$

Both with the initial condition $P_x(0) = pox$.

where;

x : vertical coordinate
w : width of opening
$w = wo - \beta \cdot x$
wo: width of opening at top
β: slope of ice edge
pox : ice pressure at top
$P_x(x)$: ice pressure in the vertical direction
note: the case number will be used
(eg case 1 : $P1_x(x)$)

K : extrusion pressure coefficient
$K = \frac{\mu_i + \mu_s}{k}$
k : lateral pressure coefficient
μ_s : ice-structure friction coefficient
μ_i : ice-ice friction coefficient
ρg : weight density of granular ice

5.3.2 Case 1 - Horizontal, Parallel Plates, with initial Pressure Px(0) = pox.

This is nominally the same simple case treated by Savage et.al in Section 5.2. The granular ice is extruded from between two parallel plates, one of steel and one of ice (Figure 18) . The centerline (left side in figure) is a symmetrical boundary, across which there is no flow. All the granular ice is extruded to the opening. The pressure at the opening is *pox*.

The differential equation is;

$$\frac{\partial P1(x)}{\partial x} + \frac{K \cdot P1_x(x)}{wo} = 0 \qquad with \quad P1_x(0) = pox \tag{29}$$

The solution to the differential equation, giving the pressure in the x direction is (see Appendix A);

$$P1_x(x) = pox \cdot e^{\left(\frac{K \cdot x}{wo}\right)} \tag{30}$$

The pressure on the plate is;

$$P1_y(x) = \frac{pox}{k} \cdot e^{\left(\frac{K \cdot x}{wo}\right)} \tag{31}$$

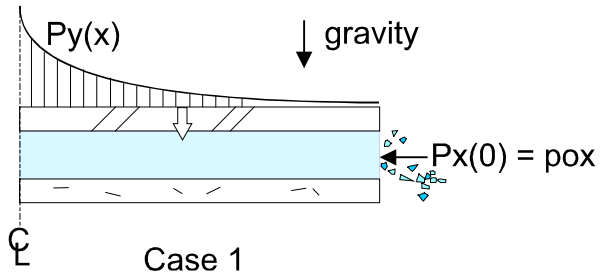

Figure 18. Case 1 - horizontal, parallel plates, with initial pressure Px(0) = pox.

Equation 22 is compared to 31 in Figure 19. In this case, it is clear that the simplified version of the equation agrees well with the more detailed model. This indicates that there is a good basis for extending the simple model to the other cases discussed below.

The Savage et.al, model starts with a nominal value of 0 for *pox*, but because of a non-zero Py (due to gravity) is able to get the integration going. In this case Py is a simple multiple of Py, so some initial value for *pox* is needed to get the integration going.

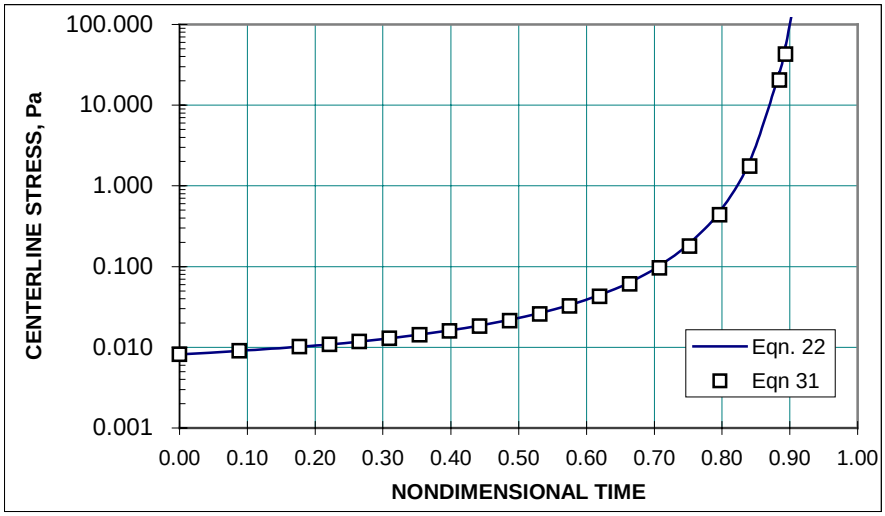

Figure 19. Comparison of Equations 22 and 31.

5.3.3 Case 2 - Vertical, Parallel Plates, with initial Pressure Px(0) = 0.

With the extrusion occuring vertically, this case adds the effect of gravity (or buoyancy) to oppose the extrusion (see Figure 20). Due to the effect of gravity, the initial pressure can be zero. The differential equation is;

$$\frac{\partial P2(x)}{\partial x} + \frac{K \cdot P2_x(x)}{wo} - \rho g = 0 \qquad with \quad P2_x(0) = 0 \tag{32}$$

The solution to the differential equation, giving the pressure in the x direction is ;

$$P2_x(x) = \rho g \cdot wo \cdot \frac{e^{\left(\frac{K \cdot x}{wo}\right)} - 1}{K} \tag{33}$$

The pressure on the plate is;

$$P2_y(x) = \rho g \cdot wo \cdot \frac{e^{\left(\frac{K \cdot x}{wo}\right)} - 1}{\mu_i + \mu_s} \tag{34}$$

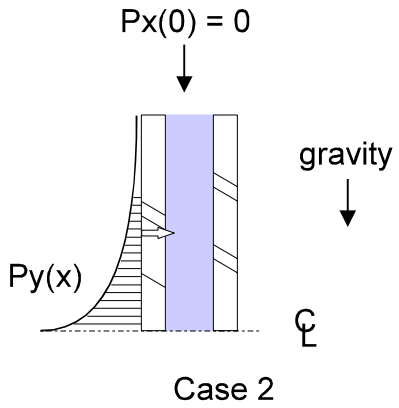

Figure 20. Case 2 Vertical, Parallel Plates, with initial Pressure Px(0) = 0.

5.3.4 Case 3 - Vertical, Sloping Plates, with initial Pressure Px(0) = 0.

Case 3 further extends the problem by considering a sloping ice face (see Figure 21). We now need a modified K , to include the effect of the opening angle on the pressure coefficient. The new constant is Ka;

$$Ka = \frac{\mu_i + \dfrac{\mu_s \cdot \cos(\beta) - \sin(\beta)}{\cos(\beta) + \mu_s \cdot \sin(\beta)}}{k} \tag{35}$$

Note that $Ka = K$ when $\beta = 0$. The differential equation is;

$$\frac{\partial P3(x)}{\partial x} + \frac{Ka \cdot P3_x(x)}{wo - \beta \cdot x} - \rho g = 0 \qquad with \quad P3_x(0) = 0 \tag{36}$$

The solution to the differential equation, giving the pressure in the x direction is ;

$$P3_x(x) = \rho g \cdot wo \cdot \frac{\rho g \cdot \left(-wo + \beta \cdot x + wo^{\left(\frac{Ka+\beta}{\beta}\right)} (wo - \beta \cdot x)^{\left(-\frac{Ka}{\beta}\right)} \right)}{Ka + \beta} \tag{37}$$

The pressure on the plate is;

$$P3_y(x) = \rho g \cdot wo \cdot \frac{\rho g \cdot \left(-wo + \beta \cdot x + wo^{\left(\frac{Ka+\beta}{\beta}\right)} (wo - \beta \cdot x)^{\left(-\frac{Ka}{\beta}\right)} \right)}{k \cdot (Ka + \beta)} \tag{38}$$

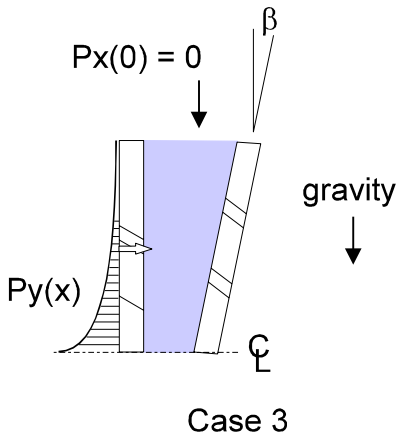

Figure 21 Case 3 Vertical, Sloping Plates, with initial Pressure Px(0) = 0.

5.3.5 Case 4 - Vertical, Parallel Plates, with initial Pressure Px(0) = pox.

This case is similar to case 2 except that the initial pressure is pox instead of zero. Figure 22 illustrates this case. The differential equation is;

$$\frac{\partial P4(x)}{\partial x} + \frac{K \cdot P4_x(x)}{wo} - \rho g = 0 \qquad with \quad P4_x(0) = 0 \tag{39}$$

The solution to the differential equation, giving the pressure in the x direction is ;

$$P4_x(x) = pox \cdot e^{\left(\frac{K \cdot x}{wo}\right)} + \rho g \cdot wo \cdot \frac{e^{\left(\frac{K \cdot x}{wo}\right)} - 1}{K} \tag{40}$$

The pressure on the plate is;

$$P4_y(x) = \frac{pox}{k} \cdot e^{\left(\frac{K \cdot x}{wo}\right)} + \rho g \cdot wo \cdot \frac{e^{\left(\frac{K \cdot x}{wo}\right)} - 1}{k \cdot K} \tag{41}$$

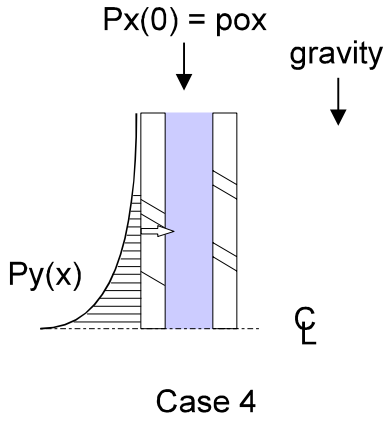

Figure 22. Case 4 Vertical, Parallel Plates, with initial Pressure Px(0) = pox.

5.3.6 Case 5 - Horizontal, Sloping Plates, with initial Pressure Px(0) = pox.

This case is similar to case 1 except with an opening angle b (see Figure 23). The differential equation is;

$$\frac{\partial P5(x)}{\partial x} + \frac{Ka \cdot P5_x(x)}{wo - \beta \cdot x} = 0 \qquad with \quad P5_x(0) = pox \tag{42}$$

with, again, Ka;

$$Ka = \frac{\mu_i + \dfrac{\mu_s \cdot \cos(\beta) - \sin(\beta)}{\cos(\beta) + \mu_s \cdot \sin(\beta)}}{k} \tag{43}$$

The solution to the differential equation, giving the pressure in the x direction is ;

$$P5_x(x) = pox \cdot (1 - \frac{\beta \cdot x}{wo})^{\left(-\frac{Ka}{\beta}\right)} \tag{44}$$

The pressure on the plate is;

$$P5_y(x) = \frac{pox}{k} \cdot (1 - \beta \cdot \frac{x}{wo})^{\left(-\frac{Ka}{\beta}\right)} \tag{45}$$

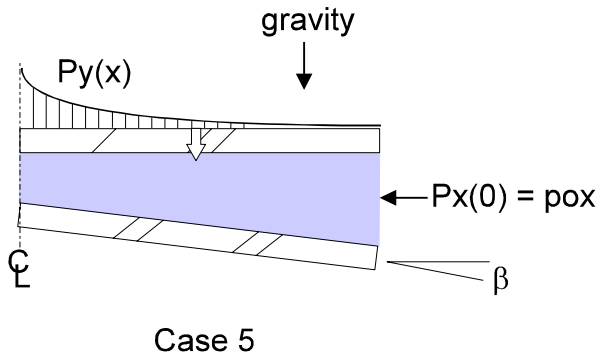

Figure 23. Case 5 Horizontal, Sloping Plates, with initial Pressure Px(0) = pox.

5.3.7 Case 6 - Vertical, Sloping Plates, with initial Pressure Px(0) = pox.

This case is similar to case 5 except that the extrusion is vertical (see Figure 24) This case represents the case closest to the true case. The differential equation is;

$$\frac{\partial P6(x)}{\partial x} + \frac{Ka \cdot P6_x(x)}{wo - \beta \cdot x} - \rho g = 0 \qquad with \quad P6_x(0) = pox \tag{46}$$

The solution to the differential equation, giving the pressure in the x direction is ;

$$P6_x(x) = \left[pox \cdot Ka \cdot (1 - \beta \cdot \frac{x}{wo})^{\left(-\frac{Ka}{\beta}\right)} + \left(pox \cdot (1 - \beta \cdot \frac{x}{wo})^{\left(-\frac{Ka}{\beta}\right)} + \rho g \cdot x \right) \cdot \beta \right.$$

$$\left. + \left((wo - \beta \cdot x)^{\left(-\frac{Ka}{\beta}\right)} \cdot wo^{\left(\frac{Ka+\beta}{\beta}\right)} - wo \right) \cdot \rho g \right] \Big/ (Ka + \beta) \tag{47}$$

The pressure on the plate is;

$$P6_y(x) = \left[pox \cdot Ka \cdot (1 - \beta \cdot \frac{x}{wo})^{\left(-\frac{Ka}{\beta}\right)} + \left(pox \cdot (1 - \beta \cdot \frac{x}{wo})^{\left(-\frac{Ka}{\beta}\right)} + \rho g \cdot x \right) \cdot \beta \right.$$

$$\left. + \left((wo - \beta \cdot x)^{\left(-\frac{Ka}{\beta}\right)} \cdot wo^{\left(\frac{Ka+\beta}{\beta}\right)} - wo \right) \cdot \rho g \right] \Big/ k(Ka + \beta) \tag{48}$$

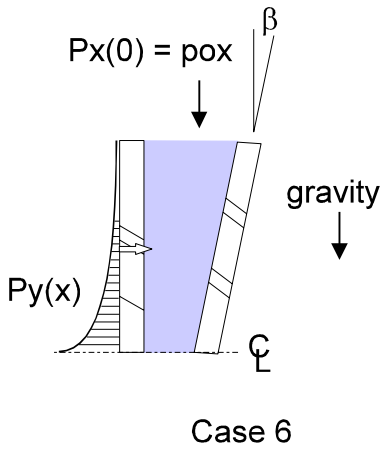

Figure 24. Case 6 Vertical, Sloping Plates, with initial Pressure Px(0) = pox.

5.3.8 Comparison and Summary

The formulae for the six cases described above are plotted on Figure 25, for the case of ;

$wo = 0.1 \cdot m$

$k = 0.4$

$\mu_i = 0.15$

$\mu_s = 0.15$

$\rho g = .0054 \cdot N / m^3$

$pox = 0.2 \cdot kPa$

$\beta = 0.1$

The case closest to our desired case is PY6. However, as it can be seen that the plots for Py5 and Py6 are almost identical, and as Py5 is a much simpler formula, the extrusion pressure will be modelled using case 5, with the formulae;

$$P5_x(x) = pox \cdot (1 - \frac{\beta \cdot x}{wo})^{\left(-\frac{Ka}{\beta}\right)} \tag{44}$$

$$P5_y(x) = \frac{pox}{k} \cdot (1 - \beta \cdot \frac{x}{wo})^{\left(-\frac{Ka}{\beta}\right)} \tag{45}$$

It can be seen that the opening angle beta has an important influence. When the plates are parallel (cases 1,2,4) the curves are straight, while when the plates are not parallel (beta >0) the curves bend upward, meaning that the pressures rise very fast. In all cases the pressures start from some initial value, which acts as a multiplier for all the pressures.

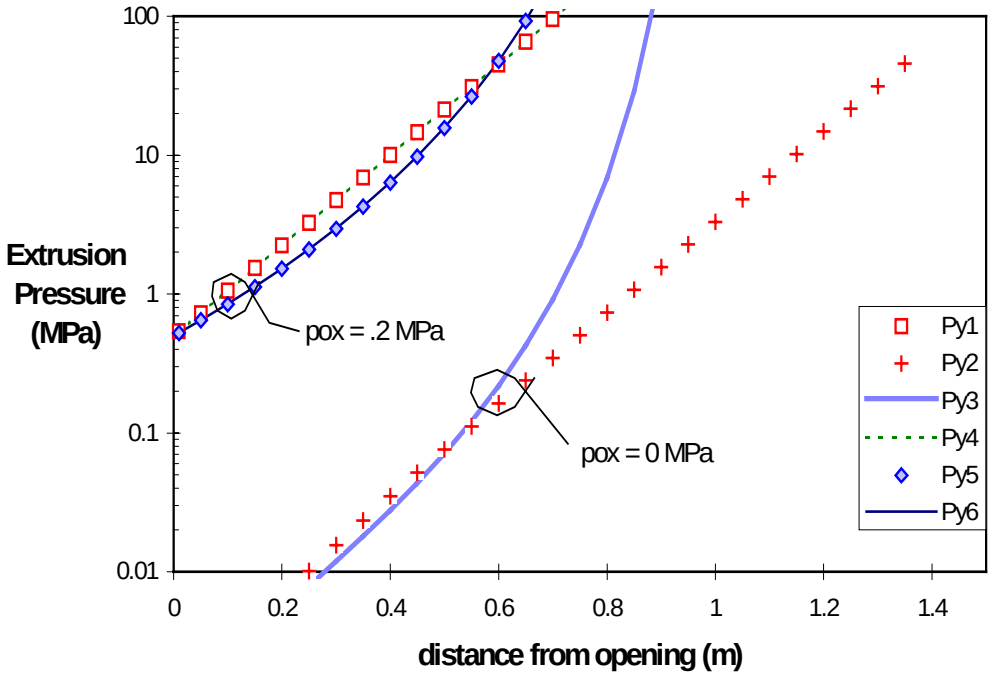

Figure 25 Comparison of Simple Extrusion Formulae

6. Discrete Ice Failure Process Model with Extrusion

The next stage in the process is to add the extrusion effects to the brittle contact model. The extrusion effects consist of two aspects; surcharge of a granular medium, and squeezing extrusion of granular medium. The granular material is assumed to have been created from all the ice removed by all prior shear flakes. Some form of comminution is assumed to have taken place, which has converted the relatively large flakes into a granular material.

The granular material is in two parts. The part above the direct contact (see Figure 26) is assumed to be dry and under the action of gravity pushing it down. The part below the direct contact is assumed to be wet and under the action of buoyancy pushing it up. Inside any static pile of granular material, there are hydrostatic pressures supporting the weight. The lateral pressures can be assumed to lateral pressure coefficient as described in the previous section.

The lateral pressures in the granular material grow very rapidly in the region close to the direct contact, and would potentially grow to be greater than the direct contact pressures. It is assumed that these high pressures would cause the granular material to re-solidify and then would behave as solid ice. A simple treatment of this issue has been implemented. It is assumed that all pressures in the granular ice are limited to the direct contact pressure. As the direct contact is assumed to be governed by the pressure to cause phase change (pressure melting), it would be unreasonable for any pressures to be above the direct contact. This issue is not of much practical importance, because neither the direct pressure, or the imposed limit have much effect on the contact forces. The main factors are the shear strength of the ice, and the passive pressures inside the granular material. Only very close to the direct contact zone do the pressures in the granular ice much exceed the passive pressures (i.o.w. gravity effects are much greater than pure extrusion effects).

The model shown in Figure 26 has been developed into two programs for calculating the contact process. The algorithm is implemented to a Maple V program (Appendix A) and a C++ program (Appendix C). The two programs are nominally the same, with the Maple version being easier to modify, while the C++ program is easier to run.

Figure 27 shows one of the plots from the Maple calculation. The two triangular regions, above and below the ice sheet, represent the accumulated granular piles of extruded ice.

Figure 28 shows one of the screens of the C++ model. In this case the orientation of contact is such that only brittle flaking (no extrusion) is taking place.

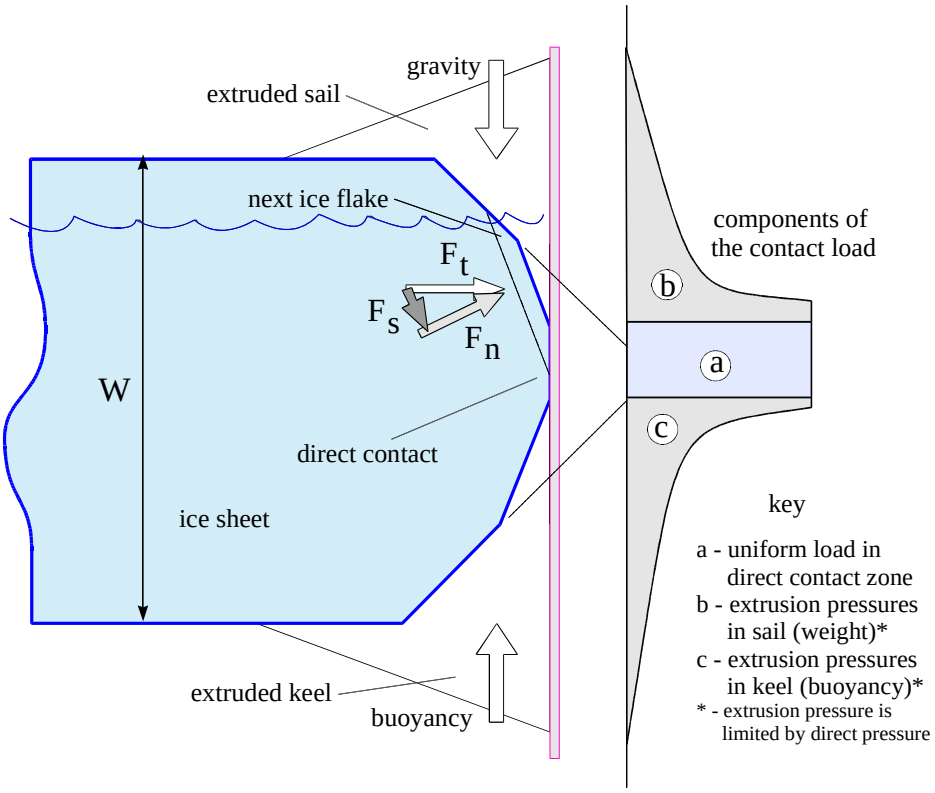

Figure 26. Brittle edge contact model with extrusion effects.

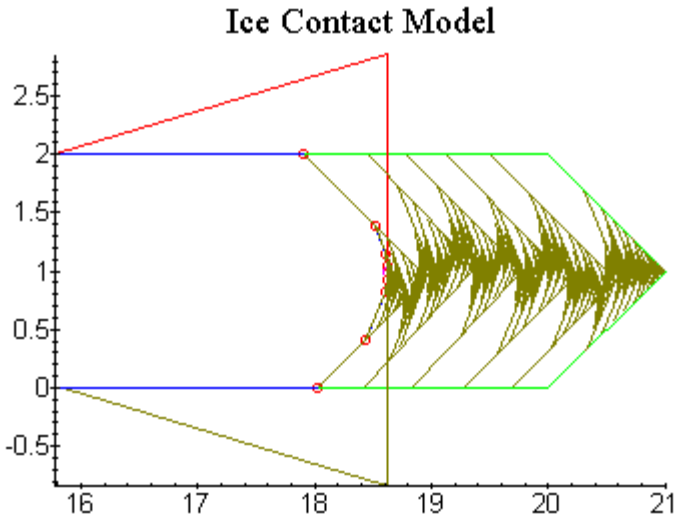

Figure 27. Plot of Maple V model after 2.4 m of penetration.

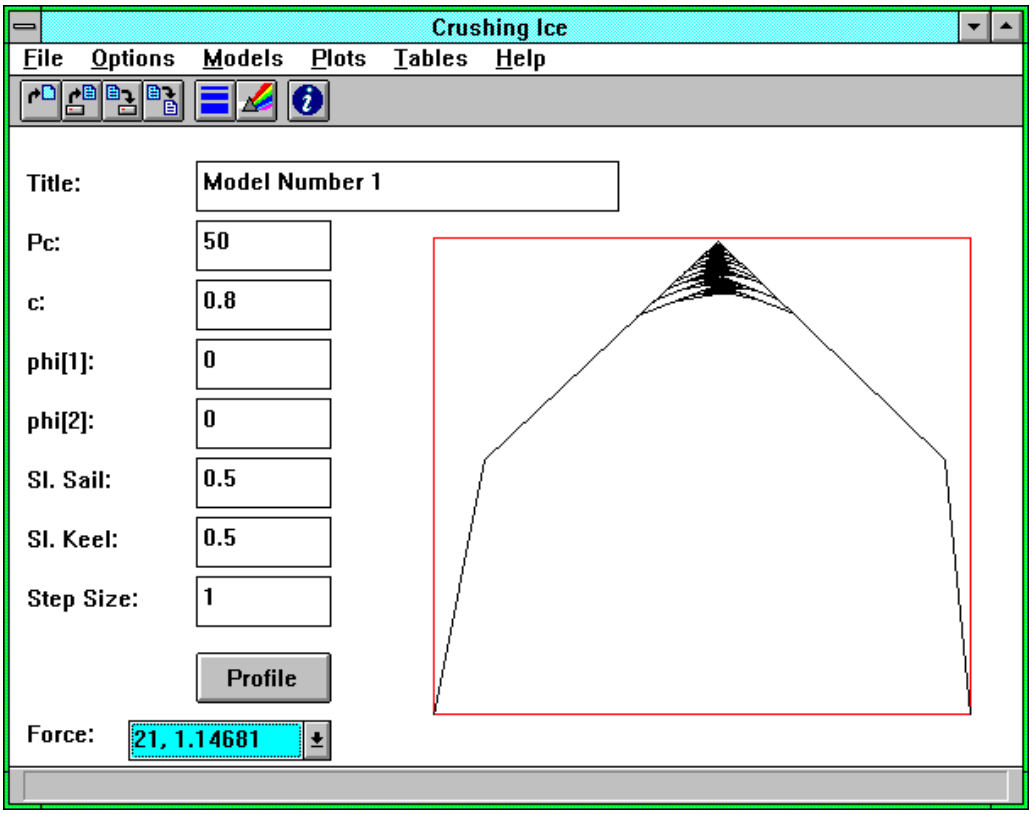

Figure 28. C++ Program Screen.

7. Results and Sensitivity

The model as described has a large number of parameters which affect the results. The main parameters are;

Table 3. Contact model parameters.

Parameter	MAPLE Variable	Typical Value
edge geometry	orig_profile	[[0,0],[0,2],[1.3],[2,2],[2,0]]
direct contact pressure	Pc	50 [MPa]
ice shear strength	c	0.8 [MPa]
Coulomb friction angle (solid ice)	Φ_1	0 deg.
friction angle (solid ice on structure)	Φ_2	0 deg
friction angle (granular ice on structure)	Φ_3	6 deg
friction angle (granular ice on solid ice)	Φ_4	10 deg
mass density of granular ice	rho	560 kg/m^3
gravity	g	9.8 m/s^2
buoyancy	gb	.12*g

The results of the model will be described in this section. The results of three runs will be presented. The parameters for the three runs are listed in Table 4. The first run is a case of only direct contact and flaking, essentially the same as the model described in (Daley, 1991). The model is two-dimensional, and so gives forces in terms of load per meter of waterline contact. The second and third runs show the effects of including the extrusion parameters, and of making a substantial change to the granular ice density and ice shear strength.

Table 4. Run Descriptions

Run Number	Description
1	Extrusion effects not included (pure flaking case)
2	Extrusion effects included with values from Table 3
3	Same as Run 2, but with Pc=20MPa, and rho=400 kg/m^3

Figure 29 shows the plot of force vs. Indentation for run #1 of the model, with only flaking (no extrusion). The ice load rises to peak at approximately 8 MN/m, with a mean level of approximately 6 MN/m. This is for an ice sheet 2m thick, a direct contact pressure of 50 Mpa (suitable for ice at -5 C), and a shear strength of 0.8 MPa. These load levels would not continue to grow with further indentation, because no rubble build-up is being modelled. The load would continue at these levels no matter how far the indentation progressed

In the case of an energy limited collision, the floe size and velocity give a kinetic energy which limits the work done by the impact. The energy consumed here is ~ 4MN x .5 m x 1/2, which is ~1 MJ /m. Given a total contact length of say 100m, and an ice floe moving at ~ 1 m/s, this corresponds to a floe mass of ~50 Mkg. Assuming a 2 m thickness, a 50 Mkg floe has dimensions of ~160m x 160m. Clearly this is not a particularly large floe. A typical floe of several kilometres across would need to crush much further to absorb the kinetic energy.

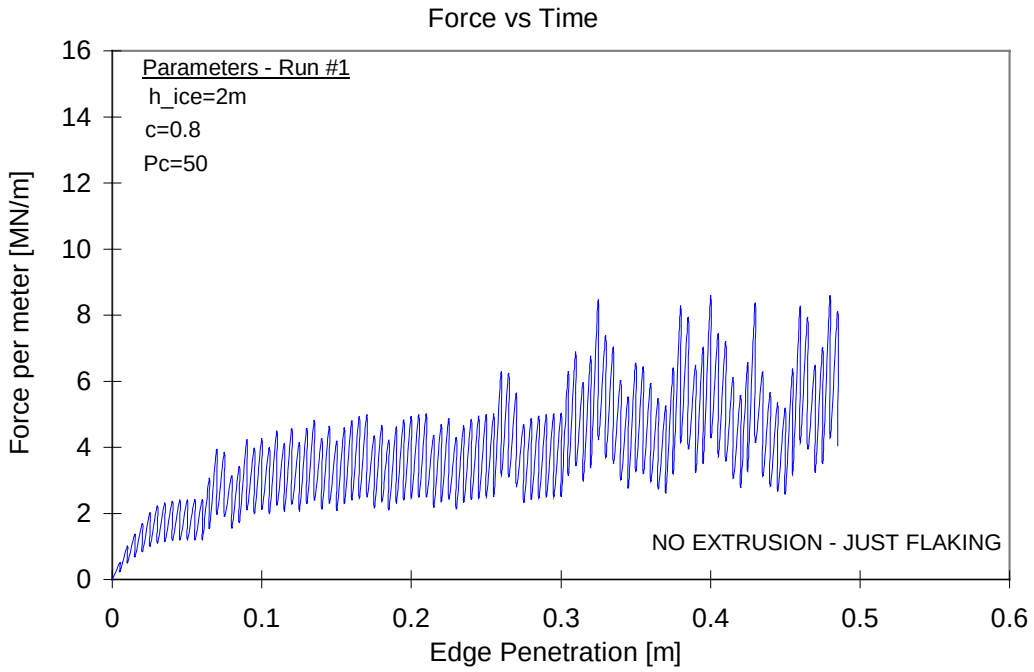

Figure 29. Force time history for Run #1 - flaking only.

Figure 30 shows the forces for run #2, which is identical to run#1 except that the effects of extrusion and rubble build-up are taken into account. The plot contains two traces. The total load is shown in the upper trace, while the load transmitted through the rubble is shown in the lower trace, which together with the direct contact form the total load.

The load in this case is significantly higher than in run #1, with peak values reaching 14 MN/m, which are almost double the values from run #1. Clearly the effect of the rubble is significant. It should also be noted that these load levels will continue to rise, because the rubble pile will continue to grow, placing greater pressures on the extruding ice, and adding even greater confinement (compressive stresses) to the incipient flakes.

The determination of maximum load values will require an analysis of how high the rubble pile can grow prior to being swept away.

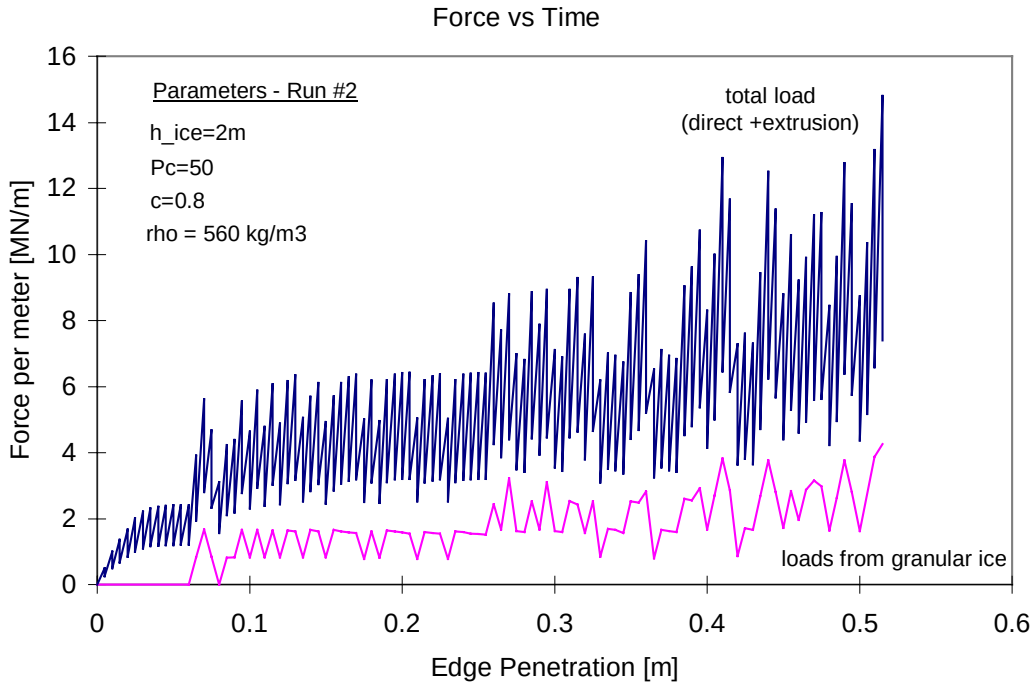

Figure 30. Force time history for Run #2 - flaking + extrusion.

Figure 31 shows the results of run #3, which includes two changes from run #2. The main change is a reduction in the mass density of the granular ice, from 560 kg/m^3 to 400 kg/m^3 . The other change is lowering the direct contact pressure to 20 MPa (from 50 MPa). The lower direct contact pressure is a secondary effect, because the direct contact force is governed by the shear strength, not the direct pressure.

The forces in run #3 are noticeably lower than run #2, but still higher than run #1. It is curious that run #3 produced a more variable force, with periods of quite low loads, and occasional spikes of high load. This system is highly non-linear, and chaotic. It is not surprising that changes in parameters can result in even qualitative changes in the load history.

It can be noticed in run #3 that the load from the granular extruding ice form a much bigger part of the total load than in earlier cases. Further analysis would be required to investigate the root causes of these behaviours.

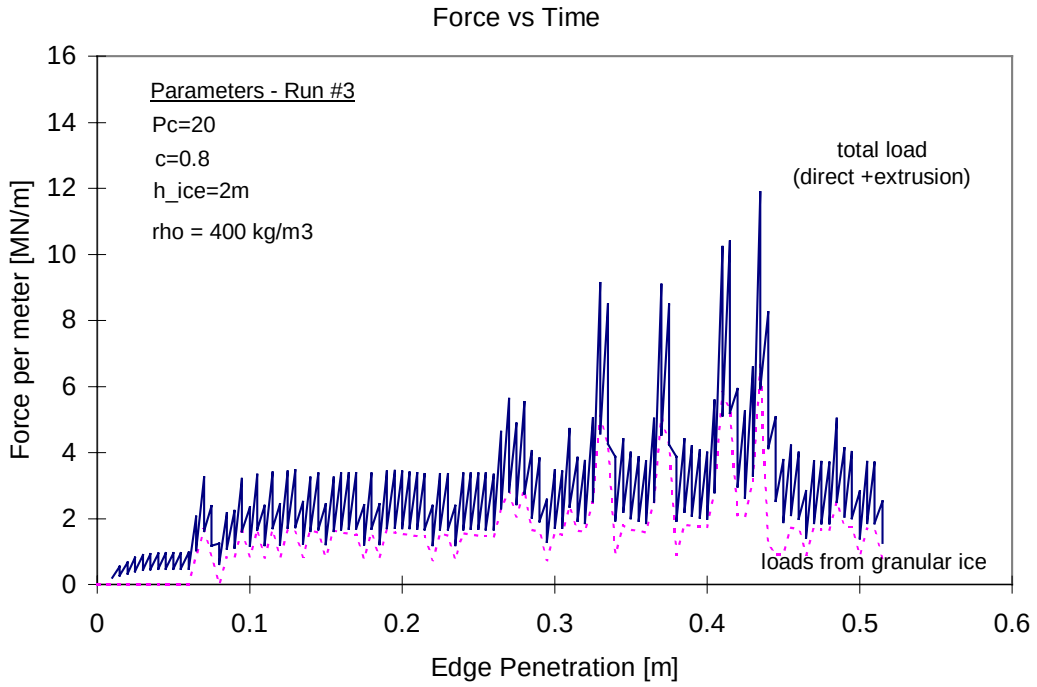

. Figure 31. Force time history for Run #3 - flaking + extrusion

Figs 29 to 31 show that the pressures from the pile of extruded rubble cause higher total loads, partly from the pressures transmitted through the granular material, and partly because the direct contact forces are higher because the pressure from the pile tends to make the cracks less likely to run (i.e. it takes a bigger direct contact before the flake occurs) This agrees with calculations by Tuhkuri (1996). It is important to realise that "squeezing" extrusion of the type found by the Savage model, is not very important. The main effects come from the fact that the extruded ice forms a pile, and then the pressures are largely a result of gravity and buoyancy (together with a lateral pressure K factor - a simple soil analogy), not "extrusion" per-se. The reasons that “extrusion” is not important are two-fold; firstly because the pressures, even between parallel plates, rise exponentially, they stay very low and then quickly jump to values high enough to solidify the ice, and secondly, in this model, the plates are not parallel, which leads to an even faster exponential rise. In a 5° wedge, the pressures say at background levels until almost at the solid contact face. Even the solidification does not itself lead to higher loads, because the combined solid+solidified contact is limited by the crack. The main issue in all this is the stress state affecting the spall crack.

8. Recommended Developments

The model shown includes a number of new features. The combination of flaking and extrusion, with the effects of rubble pile above and below the ice edge is a new development in the study of ice loads.

There are many aspects which deserve further study and enhancement. The main immediate tasks recommended are;

Further Parametric Investigation There are many variables in the model as presented. An examination of the sensitivities of the model to changes in inputs and assumptions would be quite useful. Because of the non-linear nature of the model, all the cross-sensitivities would need to be examined, which results in a very large array of cases to be run.. The most significant item to investigate is the size of the rubble pile. As the rubble pile grows the pressures increase. It may be that the resulting pressures have a significant effect on the flaking mechanics, even to the point of invalidating some of the assumptions used here.

Experimental Verification The model would benefit greatly from comparison to a set of specially designed experiments, in which an ice sheet contacts a vertical indentor. The size of the rubble pile could be artificially increased to study the effects of rubble build-up. Achieving a suitably brittle experimental ice would be the key difficulty.

The longer term developments that are needed are;

Refinement of Flaking Mechanics The mechanics of flaking, including the geometry of cracks was studied in a recent work by Tuhkuri (1995). It should be possible to include refinements to the simple cracking model given here.

Refinement of Extrusion Mechanics The model presently assumes a simple dry granular material model. It would likely be beneficial to include cohesive and viscous effects, especially for that material subject to high confinement pressures. While this report suggests that extrusion is not very important, that conclusion may change for cases where flakes do not form.

Inclusion of 3D Effects Various tests have shown that contact results in 3 dimensional effects. The pattern of direct contact is not a straight line as is assumed here. The pattern of contact is a 2D watershed pattern, and the granular ice is extruded between the ice and the structure in 3 dimensions. The experimental data available from the Medium Scale Indentor Tests (Frederking, et. al. 1990), would provide useful corroboration, but would require that the model be capable of handling 3D effects.

9. Concluding Remarks

The model presented above is a first attempt to combine a discrete flaking contact model with extrusion effects. The model shows that extrusion effects arise in two ways. Extrusion between two converging surfaces results in pressures caused largely by frictional forces inside the granular material. The rise of pressure is approximately exponential, so that the pressures toward the centre are much higher than the edge pressures. The rate of rise of pressure is increased by the opening angle. In the case presented here, the opening angles are in the range ~5 deg. To ~45 deg. In this case the pressures in the extruding wedges stay at approximately the static level, defined by gravitational effects. Only very close to the direct contact, where the gap is very small, does the pressure rise quickly to the limit pressure.

The model does show that the extruded material has a significant effect on the load levels. The main effects come from the fact that the extruded ice forms a pile, and then the pressures are largely a result of gravity and buoyancy (together with a lateral pressure K factor - a simple soil analogy), not "extrusion" per-se. The reasons that “extrusion” is not important are two-fold; firstly because the pressures, even between parallel plates, rise exponentially, they stay very low and then quickly jump to values high enough to solidify the ice, and secondly, in this model, the plates are not parallel, which leads to an even faster exponential rise. In a 5° wedge, the pressures say at background levels until almost at the solid contact face. Even the solidification does not itself lead to higher loads, because the combined solid+solidified contact is limited by the crack. The main issue in all this is the stress state affecting the spall crack.

10. References

Daley, C.G., Tuhkuri, J., and Riska, K., (1994) "The Role of Discrete Failures in Local ice Loads", Cold Regions Science and Technology. (submitted)

Daley, C. 1992, “Ice Edge Contact and Failure”, Cold Regions Science and Technology, 21 (1992) 1-23, Elsevier Science Publishers, Amsterdam.

Daley, C. 1991, “Ice Edge Contact - A Brittle Failure Process Model”, Acta Polytechnica Scandinavica, Mechanical Engineering Series No. 100, Helsinki 1991, published by the Finnish Academy of Technology.

Daley, C., 1990, “Ice Edge Contact - An Iterative Failure Process Model”, Report # M-103, Helsinki University of Technology, Laboratory of Naval Architecture.

Fransson, L., Olofsson, T., and Sandkvisk, J., 1991," Observations of the Failure Process in Ice Blocks Crushed by a Flat Indentor" Proc. of POAC 91, St. John's Canada, Sept. 24-28.

Frederking, R., Blanchet, D., Jordaan, I.J., Kennedy, K., Sinha, N.K., and Stander, E., 1990, "Field Tests of Ice Indentation at Medium Scale, Ice Island, April, 1989", National Research Council, Institute for Research in Construction, Report No. CR-5866.1, Ottawa.

Joensuu, A., Riska, K., 1988., "Jään ja Rakenteen Välinen Kosketus"(Contact Between Ice and Structure) Helsinki University of Technology, Laboratory of Naval Architecture and Marine Engineering, Report M-88, Otaniemi, 1988. (in Finnish)

Kujala, P., Goldstein, R., Osipenko, N., Danilenko, V., 1993, “A Ship in Compressive Ice - Analysis of the Ice Failure Process”, Report # M-165, Helsinki University of Technology, Ship Laboratory.

Muhonen, A., 1991 “Medium Scale Indentation Tests - PVDF pressure measurements, ice face measurements, and interpretation of crushing video”, report by Helsinki Univ. of Technology, Lab. of Naval Architecture to National Research Council of Canada.

Muhonen, A., Kärnä, T., Eranti, E., Riska, K., Järvinen, E., and Lehmus, E., 1992, "Laboratory Indentation Tests in Thick Freshwater Ice", Technical Research Centre of Finland, Research Notes 1370, Espoo, Finland.

Riska, K., Baarman, L., and Muhonen, A., 1993, “Modeling of Ice Induced Vibration of Slender Offshore Structures”, Report # M-172, Helsinki University of Technology, Arctic Offshore Research Centre.

Riska, K., Rantala, H., Joensuu, A., 1990, "Full Scale Observations of Ship-Ice Contact" Report # M-97, Helsinki University of Technology, Laboratory of Naval Architecture.

Sanderson, T.J.O., 1988, Ice Mechanics-Risks to Offshore Structures, Graham and Trotman, London

Sandwell Inc., 1992 “Reduction and Analysis of 1989 and 1990 Hobson’s Choice Ice Indentation Tests Data - Final Report”, report for Conoco, Exxon, Mobil and The National Research Council of Canada.

Savage, S.B., 1989, “Analysis of Two-dimensional Extrusion of Granular Ice Between Curved Plates”, Report to NRC, Institute for Research in Construction, NRC Contract No. 988-44174R.

Singh, S.K., Jordaan, I.J., Xiao, J., and Spencer, P.A., The Flow Properties of Crushed Ice”, the Journal of OMAE, 1995 (accepted for pulication)

Sowers, G.B., and Sowers, G.F., Introductory Soil Mechanics and Foundations, MacMillan Pub. Co., New York, 1970 (3rd ed)

Tuhkuri, J., and Riska, K., 1990, "Results from Tests on Extrusion of Crushed Ice" Report # M-98, Helsinki University of Technology, Laboratory of Naval Architecture.

Tuhkuri, J., 1994, “Analysis of Ice Fragmentation Process from Measured Particle Size Distributions of Crushed Ice”, paper accepted for publication in Journal of Cold Regions Science and Technology, Elsevier Science Publishers, Amsterdam.

Tuhkuri, J., 1996, THESIS

Appendix A: Maple Derivation and Calculation Files

Appendix B: Mathcad Simulations

Appendix C: C++ Program Listing